https://doi.org/10.5194/egusphere-2026-7081
Preprint. Discussion started: 26 November 2026
© Author(s) 2026. CC BY 4.0 License.

Atmospheric CH_4 and δ^{13}C-CH_4 trends simulated with the chemistry-climate model EMAC (version 2.55.2), Part I: Description and evaluation of the methane-flux-driven setup.

Anna-Leah Nickl[1,2], Patrick Jöckel[2], Franziska Winterstein[2], Xin Lan[3,4], Sylvia E. Michel[5,6], and Anja Schmidt[2,1]

[1]Meteorological Institute, Ludwig-Maximilians-University in Munich, Munich, Germany
[2]Institut für Physik der Atmosphäre, Deutsches Zentrum für Luft- und Raumfahrt (DLR), Oberpfaffenhofen, Germany
[3]Cooperative Institute for Research in Environmental Sciences, University of Colorado Boulder, CO, USA, 80303
[4]National Oceanic and Atmospheric Administration, Global Monitoring Laboratory, Boulder, CO, USA, 80305
[5]Institute of Arctic and Alpine Research, University of Colorado, Boulder, CO 80303
[6]Department of Atmospheric and Oceanic Sciences, University of Colorado, Boulder, CO 80303

Correspondence: Anna-Leah Nickl (anna-leah.nickl@dlr.de)

Abstract. The drivers behind the global increase of atmospheric methane (CH_4) over the last two decades remain debated. Analysing the isotopic signatures of CH_4 (δ^{13}C-CH_4 and δD-CH_4) can help to constrain individual CH_4 sources and explain the observed trend. However, several factors influence δ^{13}C-CH_4 and δD-CH_4, and therefore add uncertainty to the interpretation of the global CH_4 trend. These include the variability of individual isotopic source signatures, as well as kinetic isotopic fractionation during atmospheric CH_4 loss. Here, we present a simplified approach to simulate atmospheric CH_4 and its four main isotopologues, accounting for the influencing factors. We use the global chemistry-climate model EMAC, which calculates the basic chemical and physical processes of CH_4 and uses CH_4 emission fluxes to which we assign locally resolved δ^{13}C-CH_4 and δD-CH_4 signatures. Where these are not available, we use constant global mean signatures. The sink reactants are derived from a previously conducted interactive chemistry simulation which allowed for atmospheric feedbacks. The setup further considers the partly temperature-dependent kinetic isotopic fractionation during CH_4 oxidation and soil deposition. We evaluate our model by comparing the simulation results from 1990 to 2023 with ground-based site and globally averaged surface measurements from the NOAA Global Monitoring Laboratory. CH_4 mixing ratios are well reproduced throughout the entire time series. Refining the δ^{13}C-CH_4 source signatures gives a good overall representation of the global distribution, both meridionally and vertically. In northern high latitudes, the correlation with the observed seasonal δ^{13}C-CH_4 amplitudes is weaker, presumably due to a lack of source signature information for the predominant sources there. The trend in δ^{13}C-CH_4 from 1990–2023 is captured, but the decline after 2007 is weak, likely due to the CH_4 source composition. The simulation of δD-CH_4 shows a plausible atmospheric distribution and generally follows the observed global trend. A comprehensive analysis of δD-CH_4 is beyond the scope of this study. However, we show that effects such as fluctuating OH concentrations are discernible in the δD-CH_4 trend, making its simulation a supportive tool for interpreting the global CH_4 trend. Our work serves as a foundation for future modelling studies to investigate how sink variability and uncertainties in isotope source signatures affect global trends in CH_4, δ^{13}C-CH_4 and δD-CH_4.

https://doi.org/10.5194/egusphere-2026-7081
Preprint. Discussion started: 26 November 2026
© Author(s) 2026. CC BY 4.0 License.



Copyright statement. TEXT

1 Introduction

Atmospheric methane (CH_4) is the second most important anthropogenic greenhouse gas in terms of radiative forcing. Understanding the drivers of increasing CH_4 in the atmosphere is therefore crucial for future climate change mitigation. After a period of stagnation in the mean atmospheric CH_4 abundance between 2000 and 2007, global atmospheric mixing ratios have increased continuously to the present day. The potential causes of this new increase have been widely discussed in previous studies though with contrasting conclusions being reached. A powerful tool for evaluating the global atmospheric CH_4 budget is the analysis of the stable isotope ratios of CH_4 ($^{13}C/^{12}C$ or D/H, expressed as signatures δ^{13}C-CH_4 and δD-CH_4). The source signatures depend on their type of formation (microbial, thermogenic, pyrogenic) and can therefore be used to quantify the contribution of specific CH_4 sources to the observed atmospheric trends. Furthermore, atmospheric CH_4 sink reactions induce kinetic isotopic fractionation, which alters the isotopic composition of CH_4.

The atmospheric CH_4 rise since 2007 has been accompanied by a simultaneous decline of δ^{13}C-CH_4. Previous studies attribute the observed changes to either an increasing contribution from isotopically depleted (i.e. ^{13}C-depleted) microbial sources (Schwietzke et al., 2016; Nisbet et al., 2019; Basu et al., 2022; Oh et al., 2022; Riddell-Young et al., 2025b), or propose an equal or even greater contribution from fossil fuel emissions (Worden et al., 2017; Jackson et al., 2020; Thanwerdas et al., 2024), which are less depleted in the heavier isotope ^{13}C. In this context, a decrease of the isotopically enriched pyrogenic emissions could, for example, explain the observed decline of δ^{13}C-CH_4 (Worden et al., 2017; McNorton et al., 2018). Rigby et al. (2017) and Turner et al. (2017), in contrast, suggested that a reduced tropospheric oxidation capacity might play a role. A decrease in OH concentrations lowers CH_4 oxidation, which favours the lighter ^{12}C isotope. This reduced removal of the lighter isotope could result in a decline of δ^{13}C-CH_4 and higher CH_4 mixing ratios.

The various — and in some cases contradictory — hypotheses also highlight the complexity of modelling CH_4 and its stable isotopes. A primary challenge lies in the poorly constrained isotopic source signatures, which vary locally depending on the bulk material and further modification by kinetic isotopic fractionation during CH_4 formation and transport (Whiticar, 1999). Isotopic signatures can therefore differ within the same source categories, but also overlap between different ones, making it difficult to distinguish between them (e.g. microbial natural sources, such as wetlands and microbial anthropogenic sources, such as agriculture). Several comprehensive country- or latitude-specific data sets have been provided in recent years, which could improve their representation in global models (e.g. by Sherwood et al., 2017a; Ganesan et al., 2018; Riddell-Young et al., 2025a). The importance of applying such regional refinements is emphasized by Feinberg et al. (2018).

Another challenge lies in representing the CH_4 sink reactants in the model. Atmospheric OH is difficult to measure due to its high variability and very short lifetime (Lelieveld et al., 2004), which causes significant uncertainties in global chemistry-climate models (CCMs, Nicely et al., 2017; Zhao et al., 2020). As OH is the dominant sink of CH_4, even minor concentration changes are reflected in the CH_4 mixing ratios. However, because the isotopic fractionation associated with OH oxidation, i.e the Kinetic Isotope Effect (KIE), is small ($\varepsilon = \sim 5.4\,‰$, Cantrell et al., 1990), its impact on the global δ^{13}C-CH_4 is presumably

https://doi.org/10.5194/egusphere-2026-7081
Preprint. Discussion started: 26 November 2026
© Author(s) 2026. CC BY 4.0 License.

low. Recent studies have also emphasized the roles of chlorine (Cl) oxidation (Gromov et al., 2018; Lan et al., 2021; Basu et al., 2022; van Herpen et al., 2023) and soil consumption (Basu et al., 2022; Oh et al., 2022) in explaining the global δ^{13}C-CH_4 trend. Their KIEs are significantly stronger, with ε being 66 ‰ (Saueressig et al., 1995) and 17-18 ‰ (Snover and Quay, 2000), respectively.

A complementary approach is to analyse δD-CH_4, which provides additional constraints on the drivers of global CH_4 changes, as recently demonstrated by Riddell-Young et al. (2025b). However, sparse measurements have so far limited the application of δD-CH_4.

The aim of this paper is to present an emission-flux driven chemistry-climate model setup that is suitable for analysing factors and variability that have influenced the global CH_4 trend and its isotopic composition over the past three decades. So far, many studies have relied on box models (e.g. Schwietzke et al., 2016; Schaefer et al., 2016; Worden et al., 2017; Rigby et al., 2017; Turner et al., 2017), which utilize globally or hemispherically averaged isotopic source signatures. Furthermore, these models do not consider the spatial distribution of the sink reactants or the dynamics of stratospheric air masses, both of which may influence surface δ^{13}C-CH_4. Recent inversion frameworks based on 3-D chemistry transport models (CTMs) use sector-specific δ^{13}C-CH_4 source signatures (e.g. McNorton et al., 2018), and also consider their spatial differences (e.g., Thanwerdas et al., 2022; Basu et al., 2022). To the best of our knowledge, however, the use of spatially resolved isotopic source signatures and the additional simulation of δD-CH_4 have not yet been carried out using a CCM. Furthermore, the use of CH_4 emission fluxes in Earth system models (and CCMs) is still uncommon due to the complex feedbacks involving CH_4 in atmospheric chemistry. To date, most model setups prescribe CH_4 mixing ratios at the surface or throughout the atmosphere, and only a few studies so far have accounted for CH_4 emission fluxes in Earth system models (e.g. Folberth et al., 2022).

We use the state-of-the-art global European Centre for Medium-Range Weather Forecasts–Hamburg (ECHAM)/Modular Earth Submodel System (MESSy) Atmospheric Chemistry (EMAC) model (Jöckel et al., 2010) with a simplified approach to simulate CH_4 in the atmosphere (MESSy submodel CH4; Eichinger et al., 2015; Winterstein and Jöckel, 2021), but driven by CH_4 emission fluxes instead of prescribed lower boundary conditions. The model considers the four most abundant CH_4 isotopologues (with respect to carbon and hydrogen) and the partially temperature-dependent isotopic fractionation during physical and chemical loss of CH_4. The presented EMAC model setup utilizes recent CH_4 emission inventories and accounts for regional differences in the corresponding isotopic source signatures. We prescribe sink reactant fields derived from an earlier chemistry-climate simulation with interactive chemistry. This simplification enables computationally efficient simulations, making it suitable for a large number of sensitivity tests (Winterstein and Jöckel, 2021).

In the following, we describe the model setup including the utilized CH_4 emission flux inventories and isotopic signatures in Sect.2, and compare the simulated CH_4 and δ^{13}C-CH_4 to global surface observations and trends from 1990 to 2023 in Sect.3. Additionally, we show the simulated δD-CH_4, though data for evaluation are limited. Section 4 briefly discusses the post-stabilisation period after 2007 with respect to the emission inventories used in this setup. However, a comprehensive interpretation of the drivers of the observed trends is beyond the scope of this paper. The present study provides a detailed description and evaluation of the model, which is used in a second study to investigate and quantify possible influences on δ^{13}C-CH_4.

https://doi.org/10.5194/egusphere-2026-7081
Preprint. Discussion started: 26 November 2026
© Author(s) 2026. CC BY 4.0 License.

2 Model and simulation setup

The numerical global chemistry–climate model ECHAM/MESSy (EMAC; Jöckel et al., 2010) consists of the Modular Earth Submodel System (MESSy) coupled to the general circulation model ECHAM5 (Roeckner et al., 2006). The physics subroutines of the original ECHAM code have been modularized and reimplemented as MESSy submodels and have continuously been further developed. Only the spectral transform core, the flux-form semi-Lagrangian large scale advection scheme, and the nudging routines for Newtonian relaxation remain from ECHAM. MESSy comprises various submodels that describe different tropospheric and middle atmospheric processes, and their feedback within the climate system. The submodels which are prominent in the present study are described in the following.

2.1 Description of the applied submodels

Our setup uses the submodel CH4 (Eichinger et al., 2015; Winterstein and Jöckel, 2021) to calculate the basic chemical depletion of CH_4 and its isotopologues. It describes a simplified chemistry, which defines a CH_4 master tracer and simulates the sink processes of atmospheric CH_4, i.e. the oxidation by OH, Cl and O^1D, and the direct photolysis in the upper atmosphere. The sink reactants are provided offline as predefined fields and are not altered by the sink reactions. However, our setup employs the option of coupling the CH4 submodel to the hydrological cycle, whereby CH_4 oxidation feeds back on H_2O, more precisely on the specific humidity, which is a prognostic variable of the ECHAM model. In this way, the H_2O produced during CH_4 oxidation is taken into account, which, in turn, influences radiation and consequently affects the temperature. The photolysis rate is calculated online using the MESSy submodel JVAL (Sander et al., 2014). For the deposition in soils, EMAC uses the MESSy submodel DDEP (formerly named DRYDEP, Kerkweg et al., 2006a). In DDEP a pre-calculated deposition rate, normalized to a specific CH_4 mixing ratio of 1800 ppb (derived from Spahni et al., 2011), is prescribed and scaled to match the actual CH_4 mixing ratio per grid cell. CH_4 emission fluxes prescribed from time-dependent, gridded emission inventories (see Sect. 2.2.2) are handled by the submodel OFFEMIS (formerly named OFFLEM, Kerkweg et al., 2006b). For the radiation calculation we apply the PSrad scheme in submodel RAD (Nützel et al., 2024) with the simulated CH_4 tracer as a radiatively active species.

The CH4 submodel can further simulate the most abundant CH_4 isotopologues with respect to carbon ($^{12}CH_4$ and $^{13}CH_4$) and hydrogen (CH_4 and CH_3D). All four isotopologue tracers are subject to the same sink reactions as the master tracer. During its removal in the atmosphere, CH_4 is subject to isotopic fractionation. The lighter isotopologues $^{12}CH_4$ and CH_4 react preferentially with the oxidation partners, which leads to an enrichment of the heavier isotopologues $^{13}CH_4$ and CH_3D in the remaining methane. The degree of the fractionation and the corresponding KIE depend on the reaction rates and, therefore vary between sink reactions. For some reactions they are additionally temperature dependent. The submodel accounts for the fractionation by applying the respective KIE, which is defined as the ratio of the rate coefficients of the heavy and light isotopologues (Bigeleisen, 2005). To account for temperature dependence, the submodel calculates the KIE using the two parameters A and B

$$KIE := A \cdot exp(B/T) \tag{1}$$

https://doi.org/10.5194/egusphere-2026-7081
Preprint. Discussion started: 26 November 2026
© Author(s) 2026. CC BY 4.0 License.

with T being the temperature in K. A detailed description of the implementation of stable isotopologues in the CH4 submodel is given by Winterstein and Jöckel (2021).

Simulating only the basic CH_4 mechanisms reduces the computational demand (∼8.3 times less node hours per simulated year compared to an interactive chemistry simulation, Winterstein and Jöckel, 2021). It is therefore ideal for performing numerous sensitivity analyses in a short amount of time.

2.2 Details of the simulation setup

In this study, EMAC simulations are conducted in the T42L90MA resolution, with a spectral triangular truncation at wave number 42 (quadratic Gaussian grid of approx. 2.8° × 2.8°), and with 90 vertical hybrid pressure levels between the surface and 0.01 hPa. In order to constrain the model with the observed meteorology, we perform the simulations with "specified dynamic" (SD). EMAC is therefore nudged by Newtonian relaxation of temperature, divergence, vorticity and the logarithm of surface pressure towards the ECMWF Reanalysis version 5 data (ERA5, Hersbach et al., 2020). Relaxation times are 24 h, 48 h, 6 h, and 24 h, respectively. The relaxation is applied with a vertical profile, leaving the 3 lowermost model levels and levels above 200 hPa untouched, with transition layers of intermediate nudging strengths in between. For consistency, sea surface temperatures (SST) and sea ice concentration (SIC) to force the dynamical model have been used from ERA5 at a 12 hour frequency.

We evaluate two simulations in the present study, one spanning from January 1990 until December 2023 (SDISO-trans) and a second one branching off in January 2007 (SDISO-clim). The latter one uses a monthly climatological OH field (January–December) that is repeated cyclically after 2007. For more information on the OH fields used see Sect. 2.2.4.

2.2.1 Tracer initialization

Tracers for CH_4 and its four main stable carbon and hydrogen isotopologues are initialized with results from a previous EMAC simulation (EMAC-y-03, Frank, 2018). All tracers are scaled by a factor of 0.98 to match the observed globally averaged CH_4 mixing ratios in January 1990 (Dlugokencky et al., 2020). Additionally, $^{12}CH_4$ and $^{13}CH_4$ are adjusted to approximately fit the globally averaged δ^{13}C-CH_4 signature of -47.37 ‰ in 1990 (value taken from a historical spline of Ferretti et al. (2005), as cited by Schaefer et al., 2016).

2.2.2 Inventories of gridded CH_4 emissions fluxes

For all anthropogenic emission fluxes of CH_4, including agricultural waste burning (awb), biofuel burning and rice cultivation, we use monthly emissions from the EDGARv8.0 inventory (Crippa et al., 2023) on a 0.1° × 0.1° grid (1990–2022). Biomass burning emissions, excluding agricultural waste and biofuel burning, are taken from an optimized inventory, which was created using a Kalman filter (a posteriori emissions on a 1.0° × 1.0° grid from a previous EMAC simulation (1990–2012) performed by Frank (2018)). For the remaining period from 2012–2021 we apply biomass burning emissions on a 0.25° × 0.25° grid from the Global Fire Emissions Database, Version 4.1 (GFEDv4, Randerson et al., 2017; van der Werf et al., 2017). To account for

https://doi.org/10.5194/egusphere-2026-7081
Preprint. Discussion started: 26 November 2026
© Author(s) 2026. CC BY 4.0 License.

the effect of plume buoyancy, for example due to high temperatures of the emitted gas, anthropogenic emissions are vertically distributed and disaggregated into different emission heights, as described by Mailler et al. (2013). Similarly, biomass burning emissions are emitted at different altitudes by assigning them to the levels according to Dentener et al. (2006). Agricultural waste burning is excluded from the vertical distribution and only emitted at the surface.

Wetland emissions fluxes are derived from prognostic LPX-Bern simulations carried out for the CH_4 budget of the Global Carbon Project (GCP21, Müller/Joos pers. comm.) on a 0.5° × 0.5° grid, and are available until the year 2020. For each emission sector we repeat the last year for which data are available until the end of the simulation period in December 2023. All remaining natural emissions (i.e. termites, volcanoes, oceans and wildlife) are taken from the a posteriori inventory as described by Frank (2018), which covers the period 1990–2012. From 2012 onward we repeat the year 2012 cyclically, since we do not assume significant trends or changes (Saunois et al., 2025).

2.2.3 δ^{13}C-CH_4 and δD-CH_4 source signatures

The individual isotopic signature of CH_4 sources depends on the bulk material (i.e. the isotopic signature of the precursor organic matter) and further on the type and magnitude of its formation, which causes kinetic isotope effects (Whiticar, 1999). We account for regional environmental conditions in the setup by using a regional breakdown of δ^{13}C-CH_4, specifically for pyrogenic, wetland and fossil fuel emissions. For the latter, we also consider region-specific δD-CH_4 source signatures. The isotopic signatures are expressed relative to the isotopic standards Vienna Pee Dee Belemnite (VPDB, Werner and Brand, 2001) and Vienna Standard Ocean Water (VSMOW, Fry, 2006) for carbon and hydrogen, respectively.

For an optimal adaptation to different habitats and climatic conditions, plants have developed different pathways of carbon dioxide fixation (Ehleringer et al., 1997; Ehleringer and Cerling, 2002), resulting in different δ^{13}C-CH_4 of the bulk material. This signature can be further recognized in the CH_4 emissions from biogenic and pyrogenic sources (Dlugokencky et al., 2011). Here, we distinguish between C-3 plants (trees, crops and rice in moderate climate zones), which preferably use the lighter ^{12}C, and C-4 plants (grass and sedges in subtropical and tropical regions), which incorporate more of the heavier ^{13}C isotopes (Farquhar et al., 1989). δ^{13}C-CH_4 derived from C-3 plant material is -26 ± 3‰ for biomass burning and -70 ± 4‰ for enteric fermentation. C-4 plant-based emissions are accordingly more positive with -17 ± 3‰ and -49 ± 4‰, respectively (Dlugokencky et al., 2011). Using the map provided by Still et al. (2009) we are able to calculate a horizontal grid of isotopic signatures for all pyrogenic emissions according to the percentage of C-4 plants within the grid-box, and assume that the remaining percentage therein consists of only C-3 plants. The resulting flux-weighted transient δ^{13}C-CH_4 signatures for biomass burning emissions are presented in Fig. 1a. Signatures can deviate by more than +1.5‰ from the literature mean, but mostly remain within the range of uncertainties. They correlate with the El Niño Southern Oscillation (ENSO), i.e. negative values correspond to El Niño events, which are known to lead to enhanced biomass burning in tree-dominated (C-3 plants) regions in South America and South Asia (e.g. wildfires in Indonesia 1998), whereas, during the La Niña years emissions with a larger C-4 plant fraction occur (e.g. enhanced emissions from savanna regions in 2000, Randerson et al., 2005; Andela and van der Werf, 2014).

https://doi.org/10.5194/egusphere-2026-7081
Preprint. Discussion started: 26 November 2026
© Author(s) 2026. CC BY 4.0 License.

For livestock emissions, however, we do not assume that the source material (e.g. food for cattle) always correlates with the percentage of C-3 and C-4 plant abundance within the grid-box. Such an assumption results in flux-weighted δ^{13}C-CH_4 values that are generally much more negative than the -60.2 ‰ reported in the literature (see Supplement Fig. S2). The negative offset is comparable to the results of Feinberg et al. (2018). We therefore use a constant value for livestock emissions (see Table 1).

Next to the type of plants, the environmental conditions under which methanogenesis has taken place influence the isotopic signatures of wetlands (e.g. type of water, depth and acetate availability, Whiticar et al., 1986; Hornibrook, 2009). Moreover, kinetic fractionation may occur due to oxidation and transport through the water column and the sediment (Chanton et al., 1989). Ganesan et al. (2018) provide a spatially resolved map of wetland source signatures on a 0.5° × 0.5° grid, with typically more enriched signatures in the tropics (-56.7 ‰) and more depleted signatures in northern high latitudes (-67.8 ‰). Figure 1b shows the resulting transient flux-weighted δ^{13}C-CH_4 signatures. Besides small variabilities, they do not show a specific trend. This is consistent with findings of Poulter et al. (2017), who found only small increasing emissions from boreal wetlands and a slight decrease of tropical emissions for the period 2000–2012.

CH_4 from fossil fuels developed under high pressure and temperature conditions. The latter influences the kinetic isotopic fractionation, resulting in enriched δ^{13}C-CH_4 relative to the source rock. Moreover, δ^{13}C-CH_4 signatures depend on the source material (Whiticar, 1999). Zazzeri et al. (2016), for example, describe different coal mining source signatures ranging from low values of -70 ± 10 ‰ for sub-bituminous coals formed under low pressure and low temperature conditions, over bituminous coal with -50 ± 20 ‰, to anthracite coal formed under very high pressure and temperature conditions with higher signatures of -30 ± 10 ‰. Contrary to the biogenic sources, thermogenic sources do not show a specific latitudinal pattern. The global data set of Sherwood et al. (2017a, b) provides country-specific information for coal, gas and oil emissions. Based on this we assign each country its individual source signature. Where no source signature is available, we use a global mean signature of -41 ‰ (calculated by Frank, 2018) for coal, and -44 ‰ (Schwietzke et al., 2016) for oil and gas emissions. The transient flux-weighted δ^{13}C-CH_4 signatures fall within the mean value and uncertainty ranges reported in the literature (see Fig. 1c and 1d), with no specific trend emerging for oil and gas signatures. Coal signatures show a slight upward trend, indicating a stronger contribution from regions with isotopically enriched sources. This is presumably due to increasing emissions from China, which have relatively high isotopic source signatures. According to Thompson et al. (2015), Chinese emissions were responsible for up to 40% of the global anthropogenic CH_4 emissions from 2000–2010. However, Liu et al. (2021) suggest that Chinese emissions have slowed down since 2010 and that recent EDGAR inventories likely overestimate emissions from coal mining.

Similarly to δ^{13}C-CH_4, we assign to coal, gas and oil emissions the δD-CH_4 signatures according to the country-specific dataset from Sherwood et al. (2017a, b). Where no signatures are available, we use -140 ‰ for coal and -182.5 ‰ for gas and oil emissions as calculated in Frank (2018).

To all other CH_4 sources, we apply constant global mean δ^{13}C-CH_4 and δD-CH_4 signatures. Table 1 lists all the signatures used in the present study, including constant and flux-weighted signatures averaged over time.

https://doi.org/10.5194/egusphere-2026-7081
Preprint. Discussion started: 26 November 2026
© Author(s) 2026. CC BY 4.0 License.

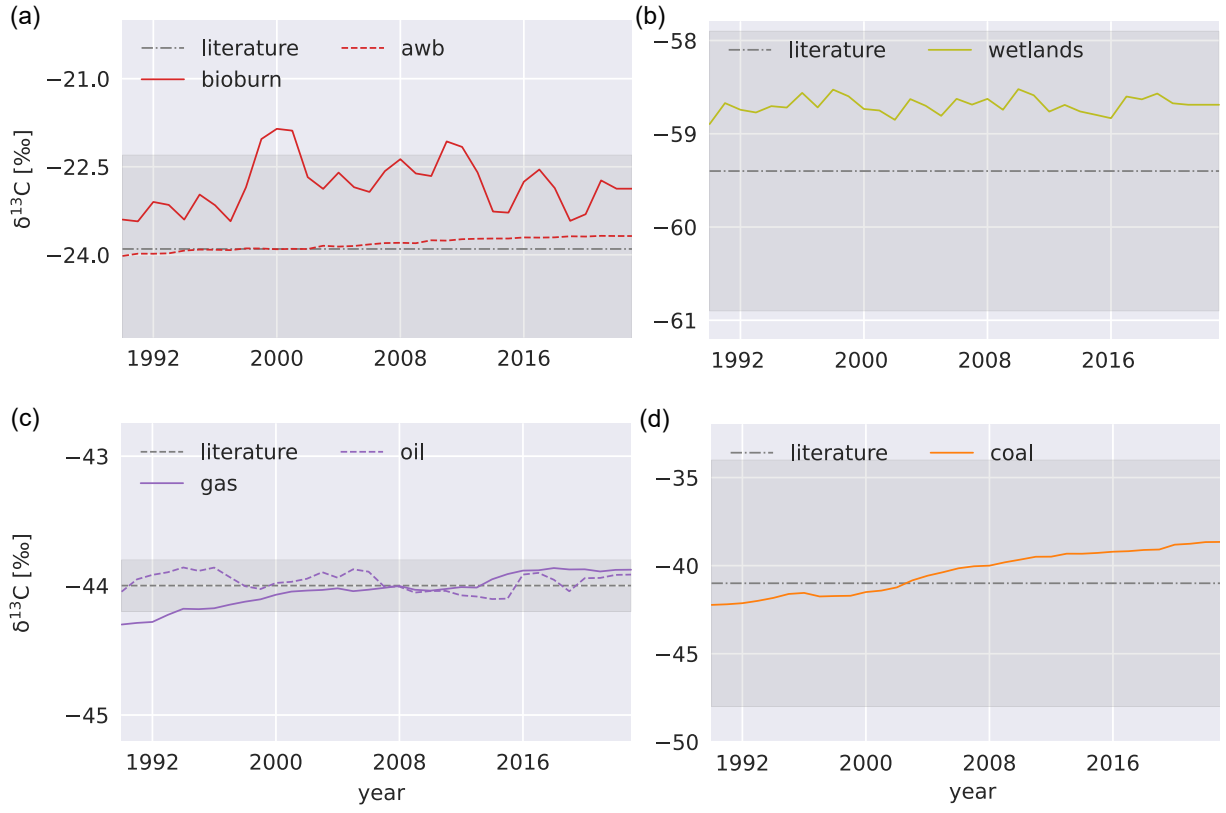


Figure 1. Transient flux-weighted δ^{13}C-CH_4 for oil and gas (purple), coal (orange), pyrogenic (red) and wetland (olive) emissions. Grey dashed lines display the corresponding mean signatures from literature as calculated by Frank (2018), and dark grey areas indicate their uncertainty range. Abbreviations: agricultural waste burning (awb), biomass burning (bioburn).

2.2.4 CH_4 sink reactants and KIEs

We prescribe pre-calculated, monthly average mixing ratios for the oxidation partners OH, Cl and O^1D. They are derived from a previous EMAC simulation (RD1-PSrad-02, Nützel et al. 2026, in prep.), which was performed with a prescribed lower boundary condition for CH_4, but with interactive chemistry, and therefore allowed atmospheric feedback on sink reactants. The mixing ratios of the sink reactants are available up to 2018. After that, monthly average mixing ratios from the most recent year are repeated until 2023 in the SDISO-trans simulation. Since the CH_4 tropospheric lifetime is comparably low in the simulation with interactive chemistry, we scale OH to result in a mean tropospheric lifetime ($\tau_{(CH_4+OH)}$) of ∼9 years between 1990–2023 (calculated as by Jöckel et al., 2006). This value matches the multi-model mean for 2000–2009 estimated by the Chemistry-Climate Model Initiative (CCMI) (Saunois et al., 2020). In the second simulation (SDISO-clim), we apply an annually repeated monthly climatology calculated from the above described transient OH field, and similarly scale it to result

https://doi.org/10.5194/egusphere-2026-7081
Preprint. Discussion started: 26 November 2026
© Author(s) 2026. CC BY 4.0 License.

Table 1. Globally averaged isotopic source signatures in [‰] used in the simulations SDISO-trans and SDISO-clim. Signatures are flux-weighted by the individual source flux and averaged over the period 1990–2023. The uncertainty corresponds to the time-series standard deviation, except for signatures adapted from Frank (2018), which utilize half the range of [Max-Min].

Source	δ^{13}C	(+/-)	Ref.	Source	δ^{13}C	(+/-)	Ref.	Source	δ^{13}C	(+/-)	Ref.
Biogenic				**Pyrogenic**				**Thermogenic**			
Wetlands	-58.7	0.5	(1)	Biomass burning	-22.8	2.0	(3,4)	Coal	-40.4	1.2	(5)
Ocean	-59.0	1.0	(2)	Awb$^{(*)}$	-23.8	0.1	(3,4)	Gas	-44.0	0.1	(5)
Termites	-63.3	6.5	(2)	- C3 (awb,bb$^{(*)}$)	-26.0	3.0	(3)	Oil	-44.0	0.1	(5)
Wildlife	-61.5	0.5	(2)	- C4 (awb,bb$^{(*)}$)	-17.0	3.0	(3)	Transport/Industry	-41.7	1.5	(2)
Livestock	-60.2	0.3	(2)	Biofuel	-23.9	1.6	(2)	Volcanoes	-40.9	0.9	(2)
Rice	-63.0	1.0	(2)								
Landfills & Wwt$^{(*)}$	-51.7	2.5	(2)								

Source	δD	(+/-)	Ref.	Source	δD	(+/-)	Ref.	Source	δD	(+/-)	Ref.
Biogenic				**Pyrogenic**				**Thermogenic**			
Wetlands	-336.2	23.8	(2)	Biomass burning	-213.0	7.5	(2)	Coal	-146.0	2.8	(5)
Ocean	-220.0	/	(2)	Awb$^{(*)}$	-213.0	7.5	(2)	Gas	-190.1	1.8	(5)
Termites	-390.0	35.5	(2)					Oil	-186.0	0.9	(5)
Wildlife	-319.0	/	(2)					Transport/Industry	-164.0	21.3	(2)
Livestock	-317.5	12.5	(2)	Biofuel	-213.0	7.5	(2)	Volcanoes	-253.4	53.5	(2)
Rice	-324.3	5.5	(2)								
Landfills & Wwt$^{(*)}$	-304.3	8.5	(2)								

[1]based on δ^{13}C map of Ganesan et al. (2018), [2]Frank (2018) and references in there,[3]Dlugokencky et al. (2011), [4]based on C3- and C4 distribution from Still et al. (2009), [5]based on dataset of Sherwood et al. (2017a, b), Awb = Agricultural waste burning, bb = Biomass burning, Wwt = Wastewater treatment

in a mean tropospheric $\tau_{(CH_4+OH)}$ of ∼9 years. The transient OH concentrations in SDISO-trans increase slightly during the considered period, resulting in a shorter mean CH_4 lifetime of ∼8.7 years between 2008–2023 (see Supplement Fig. S5).

The reported KIEs for the oxidation by OH with respect to carbon differ among several studies (Cantrell et al., 1990; Saueressig et al., 2001; Whitehill et al., 2017). We found that the value of 1.0054 from Cantrell et al. (1990) gives the best agreement with the observed δ^{13}C-CH_4 in our setup (see Supplement Fig. S2). Since $CH_4 + Cl$ fractionates strongly, a slight change to the applied chlorine field would shift the global δ^{13}C-CH_4 noticeably and, could make a different KIE for the oxidation by OH more suitable.

For all remaining sink reactions, we use KIEs as in the setup described by Winterstein and Jöckel (2021). They are additionally listed in the Supplement Table S3. The fractionation during the oxidation by OH with respect to hydrogen isotopologues depends on temperature. The same applies to oxidation by chlorine with respect to both carbon and hydrogen isotopologues.

https://doi.org/10.5194/egusphere-2026-7081
Preprint. Discussion started: 26 November 2026
© Author(s) 2026. CC BY 4.0 License.

The KIEs used are derived from Saueressig et al. (1995, 1996, 2001) and Crowley et al. (1999), and account for their temperature dependence as described above. The smallest KIE occurs for the reaction $CH_4 + O^1D$. It is not temperature dependent and taken from Saueressig et al. (2001). As shown by other studies, the fractionation during photolysis with respect to carbon isotopologues is only important in the mesosphere and the respective KIE is relatively small (e.g. by Nair et al., 2005, for the Martian atmosphere). We therefore neglect the fractionation by photolysis, similar to the setups described by Winterstein and Jöckel (2021). The KIE of photolysis with respect to hydrogen isotopologues is taken from Nair et al. (2005). The KIEs for the deposition in soil depend on the fractionation during both the diffusion into the soil and the microbial oxidation. They further vary with the type of soil, such as the soils of boreal tundra, forests or grasslands (Snover and Quay, 2000). Our setup, therefore, uses a mean KIE for deposition in soil, which is calculated from KIEs reported by Snover and Quay (2000) and Maxfield et al. (2008), or taken from Snover and Quay (2000), for carbon and hydrogen, respectively.

3 Evaluation of model results

Our model setup provides a framework in which various influences and their relative effects on the CH_4, δ^{13}C-CH_4 and δD-CH_4 trends can be investigated. This evaluation does not quantify the exact source contributions to the observed trends, but rather assesses the plausibility of the emission fluxes, isotopic source signatures and applied OH fields underlying the setup. We use monthly averaged surface observations from individual sampling sites to evaluate our model results. These sampling sites are monitored by different groups within NOAA (NOAA's Global Monitoring Laboratory) and the Institute of Arctic and Alpine Research (INSTAAR), University of Colorado, Boulder. The model output is sampled using linear interpolation at the respective NOAA location. We first show results with respect to δ^{13}C-CH_4, discussing the trends and the global distribution. Afterwards, we present our results for δD-CH_4.

3.1 Representation of CH_4 mixing ratios and δ^{13}C-CH_4 in EMAC

To evaluate the performance of our model with respect to the general evolution of CH_4 and δ^{13}C-CH_4 in the atmosphere, we also compare the simulated global averages from 1990–2023 to those from NOAA's Global Monitoring Laboratory (Michel et al., 2021; Lan et al., 2021). However, as their global means are calculated from a subset of measurements at clean marine boundary layer environments (Lan and NCAR Staff, 2025), it is difficult to make a direct comparison of the mixing ratios. Therefore, we only assess the similarity between the observed and simulated trends (Sect. 3.1.1). The subsequent Sect. 3.1.3 provides a detailed discussion on how model output, sampled at specific NOAA sites, compares to the respective surface measurements.

3.1.1 Global mean and local surface trends from 1990–2023

In general, our simulated globally averaged CH_4 mixing ratios agree well with the observed trend (Fig. 2a). The SDISO-trans simulation clearly captures the rise of the CH_4 mixing ratios until the year 2000, the subsequent stagnation period, and the renewed increase after 2007. Furthermore, similar timing and magnitude of the amplitudes suggest that the seasonal cycle is

https://doi.org/10.5194/egusphere-2026-7081
Preprint. Discussion started: 26 November 2026
© Author(s) 2026. CC BY 4.0 License.

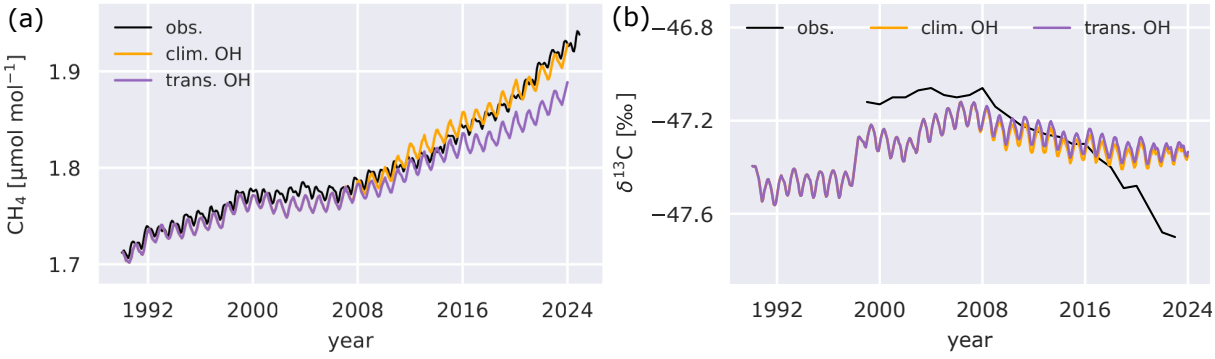


Figure 2. Simulated globally averaged surface CH_4 mixing ratios (a) and δ^{13}C-CH_4 (b), shown for the two simulations: SDISO-clim, applying a climatological OH field (yellow) and SDISO-trans, applying the transient OH field (purple), and compared to globally averaged marine surface data (black) derived from Michel et al. (2021); Lan et al. (2021); Riddell-Young et al. (2025b).

well represented. Figure 2b shows that simulated globally averaged δ^{13}C-CH_4 signatures exhibit a positive trend up until the year 2007, with a pronounced increase in 1998. A large portion of this is likely attributable to isotopically enriched wildfire emissions in Indonesia during the 1998 El Niño event (Randerson et al., 2005). The observed plateau between 2000 and 2007 is also captured by our simulation. However, the simulated global averaged δ^{13}C-CH_4 values are less positive and dropped slightly in 2002 followed by a steady increase through 2007. Since the CH_4 mixing ratios agree relatively well with the observed plateau, it is very likely that our setup does not accurately reflect the contributions of the respective sources between 2000 and 2007.

Both simulations, SDISO-trans and SDISO-clim, clearly capture the observed global increase in atmospheric CH_4 after 2007. SDISO-clim reproduces the observed trend more accurately (as also demonstrated by the comparison to local observations in the Supplement Fig. S4), showing that the observed CH_4 mixing ratios after 2007 can be achieved by using recent bottom-up emission inventories, and a stable post-2007 oxidation capacity. Our results align with the findings of Thompson et al. (2024), who suggested a stabilisation of atmospheric OH between 2004 and 2021. However, OH concentrations are one of the largest sources of uncertainty in modelling the global CH_4 budget (Zhao et al., 2020). The discrepancy between bottom-up and top-down emission estimates (Saunois et al., 2020, 2025) allows for a contrasting scenario, in which increasing CH_4 emissions are accompanied by an increase in oxidation capacity (Zhao et al., 2020; Morgenstern et al., 2025).

The observed shift towards more negative δ^{13}C-CH_4 signatures is well reproduced by both simulations, and the difference between them is rather small. Using the KIE reported by Cantrell et al. (1990), variations in OH have comparably little impact on the global δ^{13}C-CH_4 trend. Our findings are consistent with those of Lan et al. (2021) and Thanwerdas et al. (2022). In contrast, δD-CH_4 values are more affected by the oxidation with OH and result in a steeper decrease in SDISO-clim (shown later in Sect. 3.2). Including δD-CH_4 in the analyses therefore provides an additional constraint, which can be an important tool for tracking changes in OH.

https://doi.org/10.5194/egusphere-2026-7081
Preprint. Discussion started: 26 November 2026
© Author(s) 2026. CC BY 4.0 License.

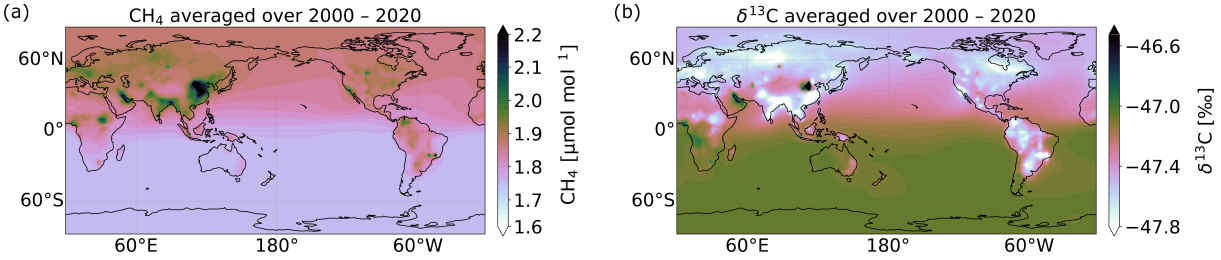


Figure 3. Simulated surface CH_4 mixing ratios (a) and δ^{13}C-CH_4 (b) averaged over the time period 2000–2020 from the "best guess" simulation.

The steep decrease in δ^{13}C-CH_4 after 2020 is not captured by our model. This is partly because emission data were not available for all sectors throughout the entire simulation period. For example, isotopically depleted wetland emissions are repeated cyclically after 2020 and an increase in these emissions would have resulted in a steeper decrease of δ^{13}C-CH_4.

We found that the simulation using the transient OH field yields reasonable CH_4 mixing ratios up until 2007. After that, the results obtained by using the climatological OH field better reflect the observed trend. The next paragraphs (Sect. 3.1.2, 3.1.3 and 3.2), therefore, analyse the model outcome based on the combination of the transient field for the period 1990–2007 and the climatological field for the period 2008–2023 as simulated by SDISO-clim. We consider this to be our "best guess" simulation.

3.1.2 Global surface, meridional and vertical distribution between 2000–2020

Figure 3 depicts the global distribution of the surface CH_4 mixing ratios and surface δ^{13}C-CH_4 signatures averaged over the time period 2000–2020 of our "best guess" simulation. We chose this time period because it covers the majority of the available continuous measurements. A discussion of the entire time series in comparison to individual site measurements is provided in the next subsection. Locally enhanced mixing ratios and the corresponding δ^{13}C-CH_4 agree well with the associated dominant CH_4 source in the respective region. Regions where high amounts of fossil-fuels are emitted, such as the South Central United States, the Persian/Arabian Gulf, or northern China, show comparatively high δ^{13}C-CH_4 values near the surface. Oil and gas hotspots can also be spotted in Canada, and the west coast of central Africa, where δ^{13}C-CH_4 near the surface is elevated. Even though eastern Europe emits high amounts of CH_4 from fossil fuel production (Kirschke et al., 2013), the δ^{13}C-CH_4 signature in this region is more depleted in the heavier isotope. One reason for this could be that CH_4 from coal mining in Upper Silesia, for example, has a comparatively low isotopic signature. Moreover, isotopic signatures might be dominated by more negative values from agriculture, i. e. in the Netherlands and the Po Valley. The Amazonas region, Siberia, South Sudan and northern Canada are dominated by isotopically depleted wetland emissions (Kirschke et al., 2013). Similarly negative signatures result from rice cultivation visible in India, Bangladesh, or China (Carlson et al., 2016), and wetlands in Southeast Asia (Kirschke et al., 2013). Low δ^{13}C-CH_4 in Brazil and the La Pampa region in Argentina could also result from intensive cattle/beef farming.

https://doi.org/10.5194/egusphere-2026-7081
Preprint. Discussion started: 26 November 2026
© Author(s) 2026. CC BY 4.0 License.

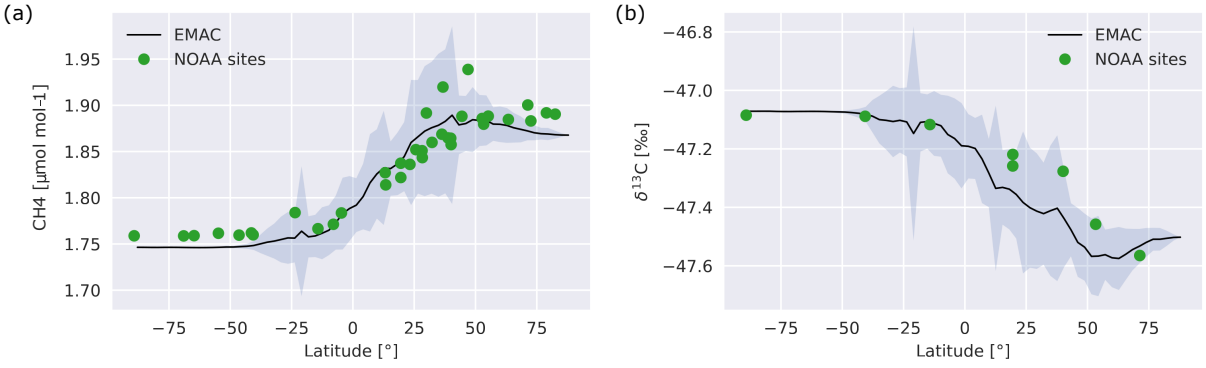


Figure 4. Zonal mean simulated CH_4 mixing ratios (a) and δ^{13}C-CH_4 (b) at surface averaged over the time period 2000–2020. The shaded area corresponds to standard deviation of the zonal mean (+/-1σ). Observational data are derived from Michel et al. (2021); Lan et al. (2021) and averaged over the same specific time period, e.g. 2000–2023. This time period has been chosen to cover a time period where most observations are available.

Overall, the regional refinement of the isotopic source signatures and the applied emission inventories result in a realistic global distribution of CH_4 mixing ratios and δ^{13}C-CH_4. CH_4 mixing ratios in Fig. 3 range from approximately 1.75 µmol mol^{-1} in the Southern Hemisphere to generally higher values of about 1.9 µmol mol^{-1} in the Northern Hemisphere. Conversely, δ^{13}C-CH_4 values decrease from around -47.1 ‰ in the south to -47.8 ‰ in the north, where the majority of CH_4 sources are located. Overall, the North-South gradient compares well with surface site measurements distributed over various latitudes (see Fig. 4). Our simulation slightly overestimates CH_4 mixing ratios in the northern high and southern high and mid latitudes. One explanation could be that the sink via OH is too low. CH_4 mixing ratios in southern mid and high latitudes mainly represent background values that are barely affected by emission sources. As δ^{13}C-CH_4 signatures are more or less consistent with the observations, it is likely that our setup closely captures the source composition contributing to the background CH_4. However, there is little measurement data available for these regions, which weakens the significance of the findings. Low and especially northern mid latitudes are most influenced by CH_4 sources. This results in higher CH_4 mixing ratios relative to the background. δ^{13}C-CH_4 signatures of the emitting sources are generally lower than the background values. This is because the latter are affected by isotopic fractionation during atmospheric removal, which leads to an isotopic enrichment of the remaining CH_4. The influence of the source can be recognized in the simulated and observed zonal gradients, which show increasing CH_4 mixing ratios and decreasing δ^{13}C-CH_4 values from south to north (see Fig. 4). Site measurements lie within the uncertainty range of the meridional mean. The wide uncertainty range reflects the variability of source strength and type in the mid latitudes. A comparison of the model results with the measurements at the specific sites is shown below.

The zonal mean gradient decreases with increasing altitude (see Fig. 5). There, mixing ratios and δ^{13}C-CH_4 are more affected by the abundance of the sink reactants. δ^{13}C-CH_4 is isotopically enriched due to the fractionation with OH in the troposphere and even more strongly by the oxidation with Cl in the stratosphere. This isotopic enrichment can be reproduced fairly well in EMAC, and δ^{13}C-CH_4 values are comparable to balloon measurements reported by Röckmann et al. (2011)

https://doi.org/10.5194/egusphere-2026-7081
Preprint. Discussion started: 26 November 2026
© Author(s) 2026. CC BY 4.0 License.

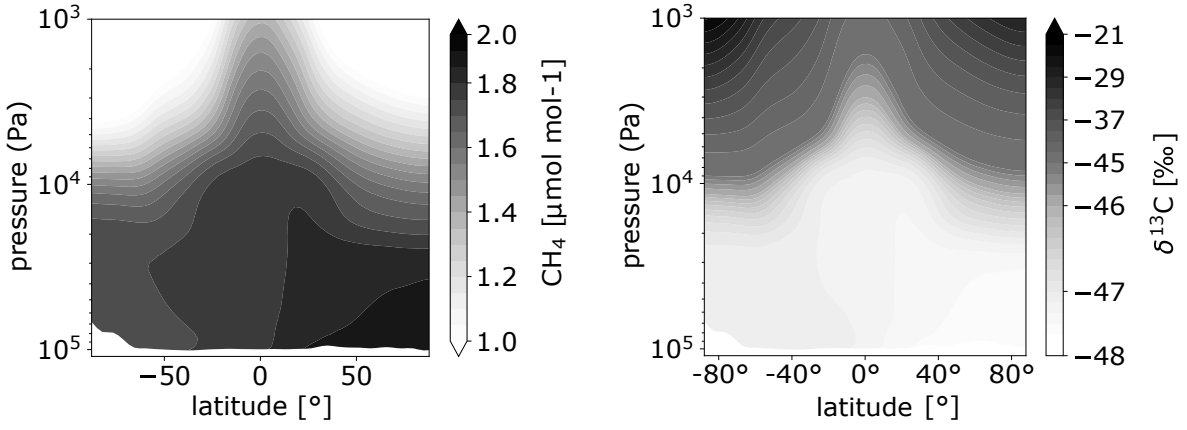


Figure 5. Simulated zonal mean vertical CH_4 mixing ratios (a) and δ^{13}C-CH_4 (b) averaged over the time period 2000–2020.

3.1.3 Comparison to individual sampling sites

By comparing individual NOAA site measurements with our model results, we aim to determine how well EMAC performs at different latitudes and in various environments. We are interested in: first, how well EMAC reproduces the observed CH_4 mixing ratios and δ^{13}C-CH_4 values; second, how well the long-term trend is reproduced; and third, to what extent the seasonal cycle matches the observations in terms of timing and amplitudes. Many observations are not available for the entire simulation period. In this case, the existing time series are compared to the corresponding period of the model results. Especially δ^{13}C-CH_4 data is sparse and only available after 1997. Sites with less than two years of continuous data are excluded from the analysis. A comparison of the time series at each site can be found in the Supplement (Fig. S6 and S7, as well as Table S4–S7).

We summarize the statistical analysis in a Taylor plot displaying the normalized standard deviation (Stdev), the centred root mean square error (RMSE) and the correlation (R) in a single diagram (see Fig. 6). The statistics are dominated by trends, which account for 88% (median across 72 stations) and 73% (median across 25 stations) of the variance for CH_4 and δ^{13}C-CH_4, respectively. To assess the bias, we calculated the RMSE of the 12-month running means. For seasonal variance, we compute the normalized Stdev of the de-trended time series, i. e. after subtracting the 12-month running mean.

Figure 6a demonstrates that the simulated CH_4 mixing ratios are generally in very good agreement with observations, with a mean (median) correlation coefficient R of 0.88 (0.97), while for the trend alone it is 0.94 (0.99), and for the seasonal variability it is 0.74 (0.82). The majority of markers are very close to, or just above, the reference line (i.e. the standard deviation is similar to that of the observations). This indicates that there is slightly higher variability in the model, which is mainly due to a steeper increase after 2007 relative to the period 2000–2007.

The model generally performs more poorly for δ^{13}C-CH_4. The mean (median) R is lower at 0.61 (0.64), with R values for trend and seasonality both being 0.63 (0.66 and 0.67). Figure 6b shows that EMAC systematically underestimates the observed variability. This is mainly due to the sharp decrease in the observed δ^{13}C-CH_4 after 2018/2020. At nearly all locations, EMAC

https://doi.org/10.5194/egusphere-2026-7081
Preprint. Discussion started: 26 November 2026
© Author(s) 2026. CC BY 4.0 License.

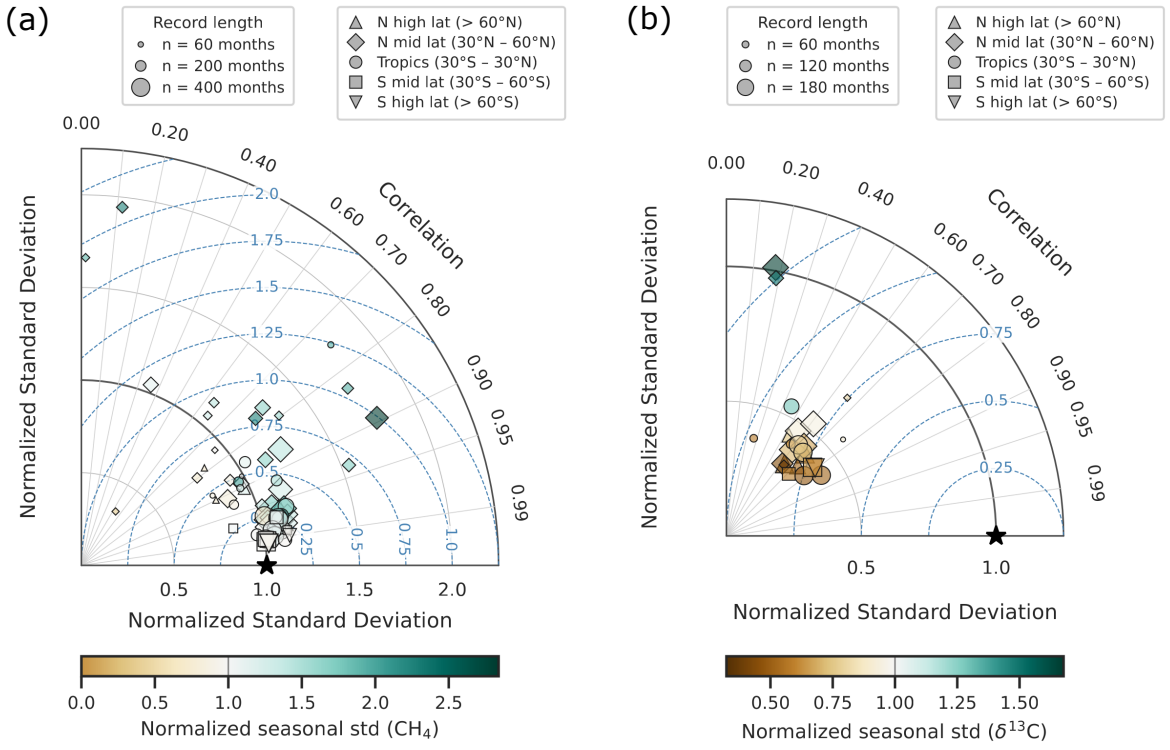


Figure 6. The Taylor diagram summarizes the statistical comparison between the simulated surface CH_4 mixing ratios (left panel) and δ^{13}C-CH_4 (right panel) with those of the observations at individual NOAA monitoring sites (between 1990–2023). Observational data are derived from Michel et al. (2021); Lan et al. (2021). The diagram shows the correlation coefficient (angle), the normalized standard deviation (radius), and the centred root mean square error (blue dotted semicircles). The black star on the horizontal axis marks the point where model results perfectly match the observations. The different markers indicate the latitude at which the sampling sites are located, and the size of the markers display the record length of the observations within the time period 1990–2023. The colour coding refers to the normalized standard deviation based on the de-trended data, illustrating the similarity of the seasonal cycles.

values stabilize or even increase after this period, resulting in a bad representation of the trend (the normalized Stdev of the trend alone is 0.28). However, the seasonal amplitudes are better reproduced than the long-term trend, with a mean normalized Stdev of 0.75, but vary from site to site.

Northern high, southern and low (pristine) latitudes

The model performs best at sites in the northern high latitudes and in the Southern Hemisphere. Many of the sites in the Southern Hemisphere are situated in pristine environments. The good agreement with the observations at these sites reveals that the well-mixed background is accurately captured. The best agreement with the observed CH_4 mixing ratios is found at both Hawaiian sites: high-altitude site Mauna Loa (MLO) and sea-level site Cape Kumukahi (KUM). Besides that, simulated

https://doi.org/10.5194/egusphere-2026-7081
Preprint. Discussion started: 26 November 2026
© Author(s) 2026. CC BY 4.0 License.

CH_4 mixing ratios are systematically lower than the observed values. This is particularly true for the period 1990–2007, during which the RMSE of the trend (12-month running mean) is approximately 28 $\pm$ 3.5 ppb in the northern high latitudes and 14 $\pm$ 3.5 ppb in the the Southern Hemisphere. After this period, mixing ratios begin to converge with the observed values, although they remain underestimated at some sites. This results in a faster increase after 2007 and slightly larger variability in the simulated trend (see Fig. 6a, where the normalized Stdev lies slightly above reference line). As already indicated by the comparison of the meridional gradient with the observations, the model setup likely overestimates the OH at high latitudes. This is also supported by the fact that δ^{13}C-CH_4 values agree comparatively well with observations. Contrary to the observed global mean, the local δ^{13}C-CH_4 time series show a small increasing trend until 2007. This is similar to the simulated δ^{13}C-CH_4 trends, and indicates that the contributions from the various emission sources are roughly the same.

The influence on the seasonal cycle is complex due to the interplay of sources, sinks and transport, especially in the Northern Hemisphere (Dlugokencky et al., 1994). As timing and magnitude of the CH_4 amplitudes match those observed at most stations (normalized seasonal Stdev close to 1), the seasonal cycle seems well represented by the model. Solely at the sites in Samoa (SMO) and Kiribati (CHR) are the simulated amplitudes significantly higher. CH_4 mixing ratios in the pristine Pacific Ocean are predominately influenced by the oxidation with OH, as local sources are sparse.

The influence on the seasonal cycle of δ^{13}C-CH_4 depends on various factors. Due to its low fractionation (Cantrell et al., 1990; Saueressig et al., 2001), it is less strongly affected by OH oxidation. δ^{13}C-CH_4 seasonality in the northern high latitudes show large variability due to transport from midlatitudes and isotopically depleted boreal wetland emissions (Quay et al., 1999; Warwick et al., 2016). The model clearly underestimates the pronounced seasonality in the northern high latitudes, although the timing of the seasonal cycle often agrees well. This could be explained by an underestimation of emissions from wetlands, a hypothesis that is contradicted by the relatively good agreement between observed and simulated CH_4 amplitudes. It is therefore more likely that our setup does not fully capture the variety of isotopic signatures of boreal wetland emissions. Here, we already use the spatially resolved map of δ^{13}C signatures of CH_4 emissions from wetlands provided by Ganesan et al. (2018). However, a study by Oh et al. (2022) suggests that considering also temporal variation in the signatures of CH_4 emissions from wetlands improves the representation of δ^{13}C-CH_4 at northern high latitudes. Further studies with EMAC could test these difference by including the data set from Oh et al. (2022) which integrates the temporal variation.

Over the Southern Ocean and in the extratropical Southern Hemisphere, δ^{13}C-CH_4 may be affected by the transport of seasonal biomass burning emissions, which are relatively enriched in the heavy isotope ^{13}C (Allan et al., 2001), or by the seasonality of chlorine in the Marine Boundary Layer (MBL) (Allan et al., 2001, 2007; Thanwerdas et al., 2022). This strong fractionation presumably causes strong variations in δ^{13}C-CH_4. The simulated δ^{13}C-CH_4 amplitudes are generally closer to observations than in the northern high latitudes, although observations often exhibit a larger inter-annual variability. At this stage we cannot determine what causes the differences between observed and simulated δ^{13}C-CH_4 values. However, the presented setup is a useful tool for testing various influences in future sensitivity studies.

Low (not pristine) and northern mid latitudes

As can be inferred from Fig. 6a, the simulated CH_4 mixing ratios again agree well with the observed mixing ratios in low and

https://doi.org/10.5194/egusphere-2026-7081
Preprint. Discussion started: 26 November 2026
© Author(s) 2026. CC BY 4.0 License.

northern mid latitudes. At most sites, we find high correlations and a normalized Stdev close to 1. Unlike the bias seen at high latitudes, the majority of the simulated CH_4 mixing ratios here show no significant offset to the observations between 1990 and 2007. Besides the previously mentioned trend deviation, the simulated δ^{13}C-CH_4 values are comparable to the observations. The amplitudes match the observed ones more closely than at high latitudes. Most sites are influenced by a combination of various emissions, including natural and anthropogenic sources. The good agreement with the observations shows that the emission inventories used in our setup produce realistic results.

Very low model performance is observed exclusively at a few sites in the northern mid latitudes. At most locations, however, the available measurements cover only a short period of time (as indicated by the size of the markers in Fig. 6), which weakens the significance of the comparisons. However, a few considerable deviations from long-term records remain. For example in Constanţa, Romania (BSC), where simulated values lie clearly below the observed CH_4 mixing ratios. Furthermore, EMAC does not reproduce the pronounced inter-annual variability at this site. The seasonal emission contribution at the BSC site is complex, with more wetland emissions from the Danube Delta in summer and emissions from fossil fuel sources prevailing in winter (Cuna et al., 2008). The interplay of both sources may not be represented properly in the simulation. However, having a continuous record of δ^{13}C-CH_4 at this site would probably help to understand the low model performance better. Similarly, simulated CH_4 amplitudes are far below the observed amplitudes in the Southern Great Plains, Oklahoma (SGP). The SGP site is highly influenced by the oil and gas industry, including unconventional gas exploitation (Maasakkers et al., 2016). Hu et al. (2025) found a strong seasonal cycle in CH_4 emissions from the oil and gas sector, where wintertime emissions are about 40% higher than those in summer. This seasonality is not reflected in the applied emission inventory.

At the NOAA site in Mongolia (UUM) and at the two sites in South Korea, Anmyeondo (AMY) and Tae-ahn Peninsula (TAP), the simulated CH_4 mixing ratios exceed the observed values from 2007 and 2008 onwards. Liu et al. (2021) found that Chinese coal emissions slowed down after 2010 and that recent EDGAR inventories likely overestimate emissions there. Zhang et al. (2025) report a shift of coal mine production to the northwestern regions, such as Inner Mongolia, which has led to an emission reduction since 2016. It is likely that the overestimation of coal mining emissions leads to the high simulated CH_4 values at the UUM site. Lee et al. (2023) describe that both sites in South Korea are influenced by local sources, such as rice cultivation, as well as by long-range transport from East Asia. The discrepancy between the simulated and observed mixing ratios at AMY and TAP might therefore also result from these too high coal mining emissions used in our setup.

3.2 Representation of δD-CH_4 in EMAC

Figure 7 illustrates the simulated global distribution of δD-CH_4 at the surface averaged over 2000–2023. This period was chosen to allow for a 10 year spin up, as we lack of proper initial conditions in 1990 (as described above). Similarly to the distribution of surface δ^{13}C-CH_4, δD-CH_4 reflects the dominant sources in different regions. Values range from -80.0 $\pm$ 2.7 ‰ (mean between 2000–2023) in the Southern Hemisphere to around -90.0 $\pm$ 4.4 ‰ in the Northern Hemisphere. Values are lower in high-emitting regions, with values down to -144 ‰. Due to the strong fractionation observed in OH oxidation with respect to hydrogen (Saueressig et al., 2001), the δD-CH_4 values are significantly higher in the south, where airmasses were longer subject to oxidation, than in regions dominated by sources. The difference of 9.8 ‰ between both hemispheres

https://doi.org/10.5194/egusphere-2026-7081
Preprint. Discussion started: 26 November 2026
© Author(s) 2026. CC BY 4.0 License.

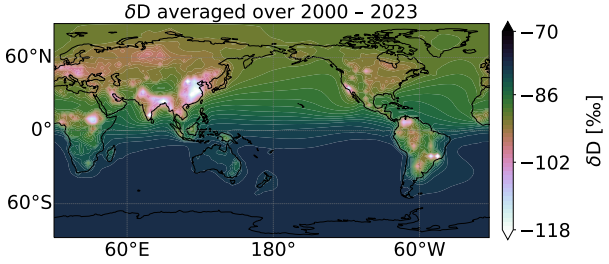


Figure 7. Simulated global δD-CH_4 surface distribution averaged over the time period 2000–2023.

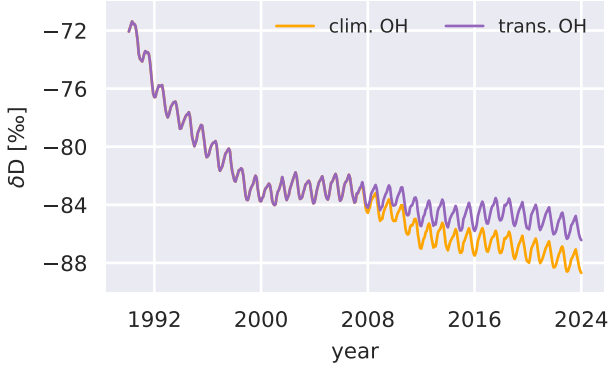


Figure 8. Simulated globally averaged surface δD-CH_4, shown for the two simulations: SDISO-clim (applying a climatological OH field) and SDISO-trans (applying the transient OH field). Sect. 3.2 evaluates the results of the "best guess" simulation, which is a combination of SDISO-trans until 2007 and SDISO-clim from 2008 onwards.

is comparable to those reported in other studies: Quay et al. (1999) found a mean difference of 10 ‰ between 1989 and 1995, and Riddell-Young et al. (2025b) recently calculated a deviation of 12 ‰ between Northern Hemisphere and Southern Hemisphere averaged over the time period 2005–2023. Since continuous measurement data and global coverage of existing data are sparse, we are unable to perform a comprehensive analysis of the simulated δD-CH_4. Nevertheless, a few data sets are available for comparison. Quay et al. (1999) reports a global mean of -86 $\pm$ 3 ‰ between 1989 and 1995. Riddell-Young et al. (2025b) provide a global mean estimate of -78.4 ‰ for the period 2005–2023. Our model's global mean for the same period lies below their value with δD-CH_4 being -85.8 $\pm$ 1.7 ‰. However, their observed decrease of 6 $\pm$ 0.8 ‰ from 2005 to 2023 is comparable to the decrease of the simulated trend (5.3 ‰, for the combined "best guess" simulation, see Fig. 8). A direct comparison with the eleven site measurements used in Riddell-Young et al. (2025b) reveals a variable model performance (see Supplement Fig. S8). While simulated δD-CH_4 is usually too light at most sites, in some regions it slightly exceeds or is very close to the observed value, such as in Syowa, Antarctica (SYO). The SYO site is unaffected by sources, which suggests that the discrepancy at other sites may result from the use of imprecise source signatures. This is not surprising, as in this set up we still lack more precise, regionally resolved δD-CH_4 signatures for the individual sources.

https://doi.org/10.5194/egusphere-2026-7081
Preprint. Discussion started: 26 November 2026
© Author(s) 2026. CC BY 4.0 License.

4 Emission fluxes contributing to post-stabilization period

As discussed in Section 3.1, we found that the decrease of δ^{13}C-CH_4 is well simulated until 2020. From 2020 onward, however, our simulations do not capture the observed sharp decrease. This is partly because we lacked emissions data at the time of performing the simulations. The following source fluxes, therefore, only refer to the period 2008–2019. In our setup, microbial emissions increased by +16.08 Tg/yr between 2008–2019 compared to the period from 2000–2007. Emissions from fossil fuel extraction increased by +17.96 Tg/yr. The simulated CH_4 mixing ratios are thus attributable to both microbial and thermogenic emissions. This is in line with findings that suggest similar or larger contributions from fossil fuel emissions (Hausmann et al., 2016; Worden et al., 2017; Jackson et al., 2020; Thanwerdas et al., 2024). On the contrary, other studies assume either a stabilization of fossil fuel emissions between 2000 and 2020 (Chandra et al., 2024), or identify microbial emissions as the main driver of the observed increase (Schwietzke et al., 2016; Schaefer et al., 2016; Nisbet et al., 2019; Basu et al., 2022; Oh et al., 2022; Riddell-Young et al., 2025b). Lan et al. (2021) also found that fossil fuel emissions are unlikely to be the main cause of the recent increase in CH_4. However, they acknowledge that uncertainties in their contribution may arise from variations in the Cl sink or from using different wetland emissions. In our setup, biomass burning emissions of CH_4 decreased by over 35% during 2008–2019 compared to 2000–2007. This probably led to the noticeable δ^{13}C-CH_4 shift, which in turn allowed for a larger contribution from fossil fuel emissions. Although recent studies report a decline of global fire activity over the last decades (Andela et al., 2017; Earl and Simmonds, 2018) and a corresponding decrease of biomass burning emissions (Worden et al., 2017), the magnitude of our emission decrease (-8.4 Tg/yr from 2008–2019 relative to 2000–2007) could be overestimated. In this case, the observed δ^{13}C-CH_4 trend would likely be driven by isotopically depleted microbial sources instead. Nevertheless, the biomass burning emissions applied in this study fall within the uncertainty ranges of the reported bottom-up inventories by Saunois et al. (2025). Hence, we believe it is worthwhile to further assess the impact of biomass burning variability on the global δ^{13}C-CH_4 trend.

5 Conclusion and Outlook

In this work we present an approach to simulate atmospheric methane (CH_4) and its stable isotopic signatures (δ^{13}C-CH_4 and δD-CH_4) using the chemistry-climate model EMAC (Jöckel et al., 2010). We applied the MESSy submodel CH4 (Eichinger et al., 2015; Winterstein and Jöckel, 2021), which calculates the basic chemical processes of CH_4, and its four main stable isotopologues, i.e. $^{12}CH_4$, $^{13}CH_4$, CH_4 and CH_3D. Furthermore, the sub-model simulates the fractionation caused by CH_4 sink reactions, taking temperature dependence into account. We prescribe the sink reactants from pre-calculated results, which are derived from an interactive chemistry simulation that accounts for atmospheric feedback on OH, Cl and O^1D. To constrain the model with the observed meteorology, EMAC is nudged towards ECMWF Reanalysis version 5 (ERA5) data. The simulations are performed in the T42L90MA resolution, and cover the time period between 1990–2023.

The novel aspect of our setup is the use of CH_4 emission fluxes and that δ^{13}C-CH_4 source signatures of emissions from wetlands, fossil fuel extraction, and the burning of biomass and agricultural waste are regionally resolved. For δD-CH_4 this was done solely to fossil fuel emissions. For all remaining sources we applied constant global mean signatures.

https://doi.org/10.5194/egusphere-2026-7081
Preprint. Discussion started: 26 November 2026
© Author(s) 2026. CC BY 4.0 License.

To evaluate the performance of our model, we compared its output to ground-based site and globally averaged surface measurements from the NOAA Global Monitoring Laboratory. This comparison showed that EMAC successfully reproduces the global surface and vertical distribution, and the meridional gradients of CH_4 and δ^{13}C-CH_4. Although we slightly overestimate CH_4 mixing ratios in the northern and southern high latitudes – potentially due to low OH concentrations – the strong overall agreement between the simulations and observations demonstrates that EMAC reliably simulates atmospheric transport, chemical loss, and isotopic fractionation.

Furthermore, the simulations capture the general course of the observed CH_4 and δ^{13}C-CH_4 trends. The best agreement for CH_4 is achieved when a constant OH field is applied after 2007 corresponding to a tropospheric CH_4 lifetime of approximately 9 years. However, variations in the OH concentration had no significant effect on the δ^{13}C-CH_4 trend, which aligns with earlier findings by Lan et al. (2021). Regardless of the applied OH field, the observed post-2007 shift in δ^{13}C-CH_4 is well represented, although not as pronounced as in the observations. In this setup, the contributions of the individual sources to the renewed increase until 2020 are comparable to those in other studies, which suggest a similar contribution from microbial and fossil fuel emissions (Worden et al., 2017; Jackson et al., 2020; Thanwerdas et al., 2024). In our model, however, the decline in isotopically enriched biomass burning emissions is considerably larger than in other estimates (Worden et al., 2017). Therefore, it is also plausible that we underestimate the contribution from isotopically depleted microbial sources, as suggested by others (Schwietzke et al., 2016; Nisbet et al., 2019; Basu et al., 2022; Oh et al., 2022; Riddell-Young et al., 2025b). However, the extent to which emissions from biomass burning and uncertainties in their source signatures affect δ^{13}C-CH_4 are a very relevant aspect in understanding the CH_4 isotopic signature and will be assessed in a second study (Part 2). Our simulations do not capture the steep post-2020 decrease in δ^{13}C-CH_4. This is partly because emission data were not available until 2023. For instance, isotopically depleted wetland emissions were repeated cyclically after 2020, whereas an actual increase would have driven a steeper decline.

The refinement of the isotope source signatures resulted in a realistic δ^{13}C-CH_4 surface distribution. Local δ^{13}C-CH_4 values correspond to the dominant sources associated with each region. The comparison of the simulation results with ground-based site measurements yields promising results regarding surface CH_4 mixing ratios. For δ^{13}C-CH_4, however, we observe weaker correlations, mainly because the trend in δ^{13}C-CH_4 after 2007 is less steep than the observed trend. Since the simulated δ^{13}C-CH_4, including intra-annual variations, agrees relatively well with the observations between 2000 and 2007, the lower correlation after 2007 is presumably caused by the composition of the sources rather than their source signatures. Moreover, the good agreement is particularly evident at sites in the northern mid latitudes, where δ^{13}C-CH_4 is influenced by various sources. However, in the northern high latitudes, the seasonal cycle of δ^{13}C-CH_4 is not accurately simulated. As the mixing ratios of CH_4 are well represented, the isotopic source signatures of wetland emissions, which predominately influence this region, may still be uncertain. Future EMAC studies should further test the influence of applying different wetland source signature inventories, such as those recently provided by Oh et al. (2022). Nevertheless, continuous measurements of δ^{13}C-CH_4 are still sparse and more data are needed to better evaluate model results.

We tested three different KIE values for OH, which are reported by Cantrell et al. (1990) Saueressig et al. (2001) and Whitehill et al. (2017), and found that the simulation using the KIE value from Cantrell et al. (1990), matches the observed

https://doi.org/10.5194/egusphere-2026-7081
Preprint. Discussion started: 26 November 2026
© Author(s) 2026. CC BY 4.0 License.

δ^{13}C-CH_4 best. However, it should be noted that δ^{13}C-CH_4 is largely influenced by the isotopic fractionation associated with Cl oxidation. As tropospheric Cl is poorly constrained in climate models, additional sensitivity studies should investigate the uncertainties induced by Cl variations.

A meaningful analysis of the simulated δD-CH_4 is hardly feasible due to a lack of source signatures information (by the time this setup was built and the simulations were conducted) and comparable observations. Nevertheless, the simulated δD-CH_4 shows a reasonable atmospheric distribution, and meridional gradients are comparable with earlier studies (Quay et al., 1999; Riddell-Young et al., 2025b). Moreover, the simulation captures the observed global trend after 2005 well. Although the performance at the few available measurement sites is highly variable, we find that general effects caused by OH sink processes can be identified in the simulated δD-CH_4. This makes the analysis of the δD-CH_4 simulated with EMAC a valuable tool for the interpretation of the global CH_4 budget. However, future simulations should include an update of the individual δD-CH_4 source signatures as recently provided by Riddell-Young et al. (2025a).

To conclude, our results provide a consistent picture for investigating the impact of sink variability or uncertainties in isotope source signatures on global CH_4 and δ^{13}C-CH_4 trends. Furthermore, using the simplified approach of simulating CH_4 using the MESSy submodel CH4 (Eichinger et al., 2015; Winterstein and Jöckel, 2021), reduces the computational time of the simulation. This enables large numbers of comprehensive sensitivity simulations to be performed using the state-of-the-art chemistry-climate model EMAC. In a second study, the setup will be used to explore the influence of atmospheric CH_4 oxidation (both by OH and Cl), soil uptake, and KIE uncertainty on the simulated global atmospheric δ^{13}C-CH_4 trend. Furthermore, we will examine its sensitivity to reduced emissions from biomass burning, which have relatively high isotopic source signatures.

Code availability. The Modular Earth Submodel System (MESSy, https://doi.org/10.5281/zenodo.8360186, MESSy Consortium, 2026) is continuously further developed and applied by a consortium of institutions. The usage of MESSy and access to the source code is licenced to all affiliates of institutions which are members of the MESSy Consortium. Institutions can become a member of the MESSy Consortium by signing the MESSy Memorandum of Understanding. Due to licence restrictions of contained legacy code, the source code can currently not be provided open source. More information can be found on the MESSy Consortium Website (http://www.messy-interface.org). The code used here (https://doi.org/10.5281/zenodo.23467434) has been based on MESSy version 2.55.2 and will be part of the next official release.

Data availability. Simulation results presented in this manuscript are available open access under https://doi.org/10.5281/zenodo.24192342.

Author contributions. ALN and PJ built the setup based on a former version, which was developed and set up by FW. ALN included the regionally resolved isotopic source signatures and performed the simulations. XL provided the CH_4 observations sampled by the NOAA's Global Monitoring Laboratory. SEM provided the stable isotope observational data from the Institute of Arctic and Alpine Research. ANL

https://doi.org/10.5194/egusphere-2026-7081
Preprint. Discussion started: 26 November 2026
© Author(s) 2026. CC BY 4.0 License.

analysed the model results based on observations and drafted the paper with input from PJ, FW and AS. The manuscript was reviewed by all authors.

Competing interests. At least one of the (co-)authors is a member of the editorial board of Geoscientific Model Development.

Acknowledgements. This work was funded by the Federal Ministry of Research, Technology and Space of Germany under the funding no. FKZ: 50EE2417 (project QuantOH). We thank Julia Marshall and Sebastian Wolff (both at DLR, Institute of Atmospheric Physics, Oberpfaffenhofen, Germany) for their helpful comments on a previous version of this paper. We further thank Fortunat Joos and Jurek Müller (both former at Climate and Environmental Physics, Physics Institute and Oeschger Centre for Climate Change Research, University of Bern, Switzerland) for providing the LPX-Bern wetland emission fluxes. We thank Owen Sherwood (Department of Earth Sciences, Dalhousie University, Halifax, Nova Scotia, Canada) et al. for the information on isotopic source signatures for coal, gas and oil emissions. We further thank the providers of the δD-CH_4 observations from specific measurement sites monitored by the Max-Planck-Institute for Biogeochemistry (MPI-BGC), Tohoku University / National Institute of Polar Research (TU/NIPR), and Institute for Marine and Atmospheric research Utrecht (IMAU), which we show in the Supplements. This work used resources of the Deutsches Klimarechenzentrum (DKRZ) granted by its Scientific Steering Committee (WLA) under project ID bd1132. Further, datasets provided by the MESSy Consortium via the DKRZ data pool were used.

https://doi.org/10.5194/egusphere-2026-7081
Preprint. Discussion started: 26 November 2026
© Author(s) 2026. CC BY 4.0 License.

References

Allan, W., Manning, M. R., Lassey, K. R., Lowe, D. C., and Gomez, A. J.: Modeling the variation of δ^{13}C in atmospheric methane: Phase ellipses and the kinetic isotope effect, Global Biogeochemical Cycles, 15, 467–481, https://doi.org/10.1029/2000GB001282, 2001.

Allan, W., Struthers, H., and Lowe, D. C.: Methane carbon isotope effects caused by atomic chlorine in the marine boundary layer: Global model results compared with Southern Hemisphere measurements, Journal of Geophysical Research: Atmospheres, 112, https://doi.org/10.1029/2006JD007369, 2007.

Andela, N. and van der Werf, G. R.: Recent trends in African fires driven by cropland expansion and El Niño to La Niña transition., Nature Clim Change, pp. 791 – 795, https://doi.org/10.1038/nclimate2313, 2014.

Andela, N., Morton, D. C., Giglio, L., Chen, Y., van der Werf, G. R., Kasibhatla, P. S., DeFries, R. S., Collatz, G. J., Hantson, S., Kloster, S., Bachelet, D., Forrest, M., Lasslop, G., Li, F., Mangeon, S., Melton, J. R., Yue, C., and Randerson, J. T.: A human-driven decline in global burned area, Science, 356, 1356–1362, https://doi.org/10.1126/science.aal4108, 2017.

Basu, S., Lan, X., Dlugokencky, E., Michel, S., Schwietzke, S., Miller, J. B., Bruhwiler, L., Oh, Y., Tans, P. P., Apadula, F., Gatti, L. V., Jordan, A., Necki, J., Sasakawa, M., Morimoto, S., Di Iorio, T., Lee, H., Arduini, J., and Manca, G.: Estimating emissions of methane consistent with atmospheric measurements of methane and δ^{13}C of methane, Atmospheric Chemistry and Physics, 22, 15 351–15 377, https://doi.org/10.5194/acp-22-15351-2022, 2022.

Bigeleisen, J.: Isotopic Effects in Chemistry and Biology, Chapter 01: Theoretical Basis of Isotope Effects from an Autobiographical Perspective, pp. 1–40, ISBN 978-0-8247-2449-8, https://doi.org/10.1201/9781420028027.ch1, 2005.

Cantrell, C. A., Shetter, R. E., McDaniel, A. H., Calvert, J. G., Davidson, J. A., Lowe, D. C., Tyler, S. C., Cicerone, R. J., and Greenberg, J. P.: Carbon kinetic isotope effect in the oxidation of methane by the hydroxyl radical, Journal of Geophysical Research: Atmospheres, 95, 22 455–22 462, https://doi.org/10.1029/JD095iD13p22455, 1990.

Carlson, K., Gerber, J., Mueller, N., Herrero, M., MacDonald, G., Brauman, K., Havlík, P., connell, C., Johnson, J., Saatchi, S., and West, P.: Greenhouse gas emissions intensity of global croplands, Nature Climate Change, 7, https://doi.org/10.1038/NCLIMATE3158, 2016.

Chandra, N., Patra, P. K., Fujita, R., Höglund-Isaksson, L., Umezawa, T., Goto, D., Morimoto, S., Vaughn, B. H., and Röckmann, T.: Methane emissions decreased in fossil fuel exploitation and sustainably increased in microbial source sectors during 1990–2020, Communications Earth & Environment, 5, 147, https://doi.org/10.1038/s43247-024-01286-x, 2024.

Chanton, J., Crill, P., Bartlett, K., and Martens, C.: Amazon Capims (floating grassmats): A source of ^{13}C enriched methane to the troposphere, Geophysical Research Letters, 16, 799–802, https://doi.org/10.1029/GL016i008p00799, 1989.

Crippa, M., Guizzardi, D., Schaaf, E., Monforti-Ferrario, F., Quadrelli, R., Risquez Martin, A., Rossi, S., Vignati, E., Muntean, M., Brandao De Melo, J., Oom, D., Pagani, F., Banja, M., Taghavi-Moharamli, P., Köykkä, J., Grassi, G., Branco, A., and San-Miguel, J.: GHG emissions of all world countries – 2023, Publications Office of the European Union, https://doi.org/10.2760/953322, 2023.

Crowley, J., Saueressig, G., Bergamaschi, P., Fischer, H., and Harris, G.: Carbon kinetic isotope effect in the reaction CH_4+Cl: a relative rate study using FTIR spectroscopy, Chemical Physics Letters, 303, 268–274, https://doi.org/10.1016/S0009-2614(99)00243-2, 1999.

Cuna, S., Pendall, E., Miller, J. B., Tans, P. P., Dlugokencky, E., and White, J. W.: Separating contributions from natural and anthropogenic sources in atmospheric methane from the Black Sea region, Romania, Applied Geochemistry, 23, 2871–2879, https://doi.org/10.1016/j.apgeochem.2008.04.019, special Issue AIG-6, 2008.

Dentener, F., Kinne, S., Bond, T., Boucher, O., Cofala, J., Generoso, S., Ginoux, P., Gong, S., Hoelzemann, J. J., Ito, A., Marelli, L., Penner, J. E., Putaud, J.-P., Textor, C., Schulz, M., van der Werf, G. R., and Wilson, J.: Emissions of primary aerosol and precursor gases in the

https://doi.org/10.5194/egusphere-2026-7081
Preprint. Discussion started: 26 November 2026
© Author(s) 2026. CC BY 4.0 License.

years 2000 and 1750 prescribed data-sets for AeroCom, Atmospheric Chemistry and Physics, 6, 4321–4344, https://doi.org/10.5194/acp-6-4321-2006, 2006.

Dlugokencky, E., Crotwell, A., Mund, J., Crotwell, M., and Thoning, K.: Atmospheric Methane Dry Air Mole Fractions from the NOAA GML Carbon Cycle Cooperative Global Air Sampling Network, 1983-2019, Version: 2020-07, https://doi.org/10.15138/VNCZ-M766, 2020.

Dlugokencky, E. J., Steele, L. P., Lang, P. M., and Masarie, K. A.: The growth rate and distribution of atmospheric methane, Journal of Geophysical Research: Atmospheres, 99, 17 021–17 043, https://doi.org/10.1029/94JD01245, 1994.

Dlugokencky, E. J., Nisbet, E. G., Fisher, R., and Lowry, D.: Global atmospheric methane: budget, changes and dangers, Philosophical Transactions of the Royal Society A: Mathematical, Physical and Engineering Sciences, 369, 2058–2072, https://doi.org/10.1098/rsta.2010.0341, 2011.

Earl, N. and Simmonds, I.: Spatial and Temporal Variability and Trends in 2001–2016 Global Fire Activity, Journal of Geophysical Research: Atmospheres, 123, 2524–2536, https://doi.org/10.1002/2017JD027749, 2018.

Ehleringer, J. and Cerling, T.: C3 and C4 Photosynthesis, Encyclopedia of Global Environmental Change, 2, 2002.

Ehleringer, J., Cerling, T., and Helliker, B.: C-4 photosynthesis, atmospheric CO_2 and climate, Oecologia, 112, 285–299, https://doi.org/10.1007/s004420050311, 1997.

Eichinger, R., Jöckel, P., Brinkop, S., Werner, M., and Lossow, S.: Simulation of the isotopic composition of stratospheric water vapour – Part 1: Description and evaluation of the EMAC model, Atmospheric Chemistry and Physics, 15, 5537–5555, https://doi.org/10.5194/acp-15-5537-2015, 2015.

Farquhar, G. D., Ehleringer, J. R., and Hubick, K. T.: Carbon Isotope Discrimination and Photosynthesis, Annual Review of Plant Physiology and Plant Molecular Biology, 40, 503–537, https://doi.org/10.1146/annurev.pp.40.060189.002443, 1989.

Feinberg, A. I., Coulon, A., Stenke, A., Schwietzke, S., and Peter, T.: Isotopic source signatures: Impact of regional variability on the $\delta^{13}CH_4$ trend and spatial distribution, Atmospheric Environment, 174, 99 – 111, https://doi.org/10.1016/j.atmosenv.2017.11.037, 2018.

Ferretti, D. F., Miller, J. B., White, J. W. C., Etheridge, D. M., Lassey, K. R., Lowe, D. C., Meure, C. M. M., Dreier, M. F., Trudinger, C. M., van Ommen, T. D., and Langenfelds, R. L.: Unexpected Changes to the Global Methane Budget over the Past 2000 Years, Science, 309, 1714–1717, https://doi.org/10.1126/science.1115193, 2005.

Folberth, G. A., Staniaszek, Z., Archibald, A. T., Gedney, N., Griffiths, P. T., Jones, C. D., O'Connor, F. M., Parker, R. J., Sellar, A. A., and Wiltshire, A.: Description and Evaluation of an Emission-Driven and Fully Coupled Methane Cycle in UKESM1, Journal of Advances in Modeling Earth Systems, 14, e2021MS002 982, https://doi.org/10.1029/2021MS002982, 2022.

Frank, F. I.: Atmospheric methane and its isotopic composition in a changing climate, Ph.D. thesis, Ludwig-Maximilians-Universität München, https://doi.org/10.5282/edoc.22578, 2018.

Fry, B.: Isotope Notation and Measurement. In: Stable Isotope Ecology. Springer, New York, NY. https://doi.org/10.1007/0-387-33745-8_2, ISBN 978-0-387-30513-4, https://doi.org/10.1007/0-387-33745-8_2, 2006.

Ganesan, A. L., Stell, A. C., Gedney, N., Comyn-Platt, E., Hayman, G., Rigby, M., Poulter, B., and Hornibrook, E. R. C.: Spatially Resolved Isotopic Source Signatures of Wetland Methane Emissions, Geophysical Research Letters, 45, 3737–3745, https://doi.org/10.1002/2018GL077536, 2018.

Gromov, S., Brenninkmeijer, C. A. M., and Jöckel, P.: A very limited role of tropospheric chlorine as a sink of the greenhouse gas methane, Atmospheric Chemistry and Physics, 18, 9831–9843, https://doi.org/10.5194/acp-18-9831-2018, 2018.

https://doi.org/10.5194/egusphere-2026-7081
Preprint. Discussion started: 26 November 2026
© Author(s) 2026. CC BY 4.0 License.

Hausmann, P., Sussmann, R., and Smale, D.: Contribution of oil and natural gas production to renewed increase in atmospheric methane (2007–2014): top–down estimate from ethane and methane column observations, Atmospheric Chemistry and Physics, 16, 3227–3244, https://doi.org/10.5194/acp-16-3227-2016, 2016.

Hersbach, H., Bell, B., Berrisford, P., Hirahara, S., Horányi, A., Muñoz-Sabater, J., Nicolas, J., Peubey, C., Radu, R., Schepers, D., Simmons, A., Soci, C., Abdalla, S., Abellan, X., Balsamo, G., Bechtold, P., Biavati, G., Bidlot, J., Bonavita, M., De Chiara, G., Dahlgren, P., Dee, D., Diamantakis, M., Dragani, R., Flemming, J., Forbes, R., Fuentes, M., Geer, A., Haimberger, L., Healy, S., Hogan, R. J., Hólm, E., Janisková, M., Keeley, S., Laloyaux, P., Lopez, P., Lupu, C., Radnoti, G., de Rosnay, P., Rozum, I., Vamborg, F., Villaume, S., and Thépaut, J.-N.: The ERA5 global reanalysis, Quarterly Journal of the Royal Meteorological Society, 146, 1999–2049, https://doi.org/10.1002/qj.3803, 2020.

Hornibrook, E.: The Stable Carbon Isotope Composition of Methane Produced and Emitted from Northern Peatlands, Washington DC American Geophysical Union Geophysical Monograph Series, 184, 187–203, https://doi.org/10.1029/2008GM000828, 2009.

Hu, L., Andrews, A. E., Montzka, S. A., Miller, S. M., Bruhwiler, L., Oh, Y., Sweeney, C., Miller, J. B., McKain, K., Ibarra Espinosa, S., Davis, K., Miles, N., Mountain, M., Lan, X., Crotwell, A., Madronich, M., Mefford, T., Michel, S., and Houwelling, S.: An Unexpected Seasonal Cycle in U.S. Oil and Gas Methane Emissions, Environmental Science & Technology, 59, 9968–9979, https://doi.org/10.1021/acs.est.4c14090, 2025.

Jackson, R. B., Saunois, M., Bousquet, P., Canadell, J. G., Poulter, B., Stavert, A. R., Bergamaschi, P., Niwa, Y., Segers, A., and Tsuruta, A.: Increasing anthropogenic methane emissions arise equally from agricultural and fossil fuel sources, Environmental Research Letters, 15, 071 002, https://doi.org/10.1088/1748-9326/ab9ed2, 2020.

Jöckel, P., Tost, H., Pozzer, A., Brühl, C., Buchholz, J., Ganzeveld, L., Hoor, P., Kerkweg, A., Lawrence, M. G., Sander, R., Steil, B., Stiller, G., Tanarhte, M., Taraborrelli, D., van Aardenne, J., and Lelieveld, J.: The atmospheric chemistry general circulation model ECHAM5/MESSy1: consistent simulation of ozone from the surface to the mesosphere, Atmospheric Chemistry and Physics, 6, 5067–5104, https://doi.org/10.5194/acp-6-5067-2006, 2006.

Jöckel, P., Kerkweg, A., Pozzer, A., Sander, R., Tost, H., Riede, H., Baumgaertner, A., Gromov, S., and Kern, B.: Development cycle 2 of the Modular Earth Submodel System (MESSy2), Geoscientific Model Development, 3, 717–752, https://doi.org/10.5194/gmd-3-717-2010, 2010.

Kerkweg, A., Buchholz, J., Ganzeveld, L., Pozzer, A., Tost, H., and Jöckel, P.: Technical Note: An implementation of the dry removal processes DRY DEPosition and SEDImentation in the Modular Earth Submodel System (MESSy), Atmospheric Chemistry and Physics, 6, 4617–4632, https://doi.org/10.5194/acp-6-4617-2006, 2006a.

Kerkweg, A., Sander, R., Tost, H., and Jöckel, P.: Technical note: Implementation of prescribed (OFFLEM), calculated (ONLEM), and pseudo-emissions (TNUDGE) of chemical species in the Modular Earth Submodel System (MESSy), Atmospheric Chemistry and Physics, 6, 3603–3609, https://doi.org/10.5194/acp-6-3603-2006, 2006b.

Kirschke, S., Bousquet, P., Ciais, P., Saunois, M., Canadell, J., Dlugokencky, E., Bergamaschi, P., Bergmann, D., Blake, D., Bruhwiler, L., Cameron-Smith, P., Castaldi, S., Chevallier, F., Feng, L., Fraser, A., Heimann, M., Hodson, E., Houweling, S., Josse, B., and Zeng, G.: Three decades of global methane sources and sinks, Nature Geoscience, 6, 813–823, https://doi.org/10.1038/ngeo1955, 2013.

Lan, X. and NCAR Staff: The Climate Data Guide: Global-mean methane at the Earth's surface from NOAA's global cooperative greenhouse gas measurements, Climate Data Guide, UCAR/NCAR, https://climatedataguide.ucar.edu/climate-data/global-mean-methane-earths-surface-noaas-global-cooperative-greenhouse-gas, last modified: 2025-12-11, last accessed: 2026-05-27, 2025.

https://doi.org/10.5194/egusphere-2026-7081
Preprint. Discussion started: 26 November 2026
© Author(s) 2026. CC BY 4.0 License.

Lan, X., Basu, S., Schwietzke, S., Bruhwiler, L. M. P., Dlugokencky, E. J., Michel, S. E., Sherwood, O. A., Tans, P. P., Thoning, K., Etiope, G., Zhuang, Q., Liu, L., Oh, Y., Miller, J. B., Pétron, G., Vaughn, B. H., and Crippa, M.: Improved Constraints on Global Methane Emissions and Sinks Using δ^{13}C-CH_4, Global Biogeochemical Cycles, 35, e2021GB007 000, https://doi.org/10.1029/2021GB007000, 2021.

Lee, H., Seo, W., Li, S., Lee, S., Kenea, S. T., and Joo, S.: Measurement report: Atmospheric CH_4 at regional stations of the Korea Meteorological Administration–Global Atmosphere Watch Programme: measurement, characteristics, and long-term changes of its drivers, Atmospheric Chemistry and Physics, 23, 7141–7159, https://doi.org/10.5194/acp-23-7141-2023, 2023.

Lelieveld, J., Dentener, F. J., Peters, W., and Krol, M. C.: On the role of hydroxyl radicals in the self-cleansing capacity of the troposphere, Atmospheric Chemistry and Physics, 4, 2337–2344, https://doi.org/10.5194/acp-4-2337-2004, 2004.

Liu, G., Peng, S., Lin, X., Ciais, P., Li, X., Xi, Y., Lu, Z., Chang, J., Saunois, M., Wu, Y., Patra, P., Chandra, N., Zeng, H., and Piao, S.: Recent Slowdown of Anthropogenic Methane Emissions in China Driven by Stabilized Coal Production, Environmental Science & Technology Letters, 8, 739–746, https://doi.org/10.1021/acs.estlett.1c00463, 2021.

Maasakkers, J. D., Jacob, D. J., Sulprizio, M. P., Turner, A. J., Weitz, M., Wirth, T., Hight, C., DeFigueiredo, M., Desai, M., Schmeltz, R., Hockstad, L., Bloom, A. A., Bowman, K. W., Jeong, S., and Fischer, M. L.: Gridded National Inventory of U.S. Methane Emissions, Environmental Science & Technology, 50, 13 123–13 133, https://doi.org/10.1021/acs.est.6b02878, pMID: 27934278, 2016.

Mailler, S., Khvorostyanov, D., and Menut, L.: Impact of the vertical emission profiles on background gas-phase pollution simulated from the EMEP emissions over Europe, Atmospheric Chemistry and Physics, 13, 5987–5998, https://doi.org/10.5194/acp-13-5987-2013, 2013.

Maxfield, P. J., Evershed, R. P., and Hornibrook, E. R. C.: Physical and Biological Controls on the In Situ Kinetic Isotope Effect Associated with Oxidation of Atmospheric CH_4 in Mineral Soils, Environmental Science & Technology, 42, 7824–7830, https://doi.org/10.1021/es800544q, 2008.

McNorton, J., Wilson, C., Gloor, M., Parker, R. J., Boesch, H., Feng, W., Hossaini, R., and Chipperfield, M. P.: Attribution of recent increases in atmospheric methane through 3-D inverse modelling, Atmospheric Chemistry and Physics, 18, 18 149–18 168, https://doi.org/10.5194/acp-18-18149-2018, 2018.

MESSy Consortium: The Modular Earth Submodel System, https://doi.org/10.5281/zenodo.8360186, 2026.

Michel, S. E., Vaughn, B. H., Tans, P. P., Thoning, K., and Lan, X.: Atmospheric d13C-CH4 data from the Institute of Arctic and Alpine Research (INSTAAR) at the University of Colorado, Boulder in cooperation with NOAA Global Monitoring Laboratory [data set], https://doi.org/10.15138/79jq-qc24, accessed in 2025, 2021.

Morgenstern, O., Moss, R., Manning, M., Zeng, G., Schaefer, H., Usoskin, I., Turnbull, J., Brailsford, G., Nichol, S., and Bromley, T.: Radiocarbon monoxide indicates increasing atmospheric oxidizing capacity, Nature Communications, 16, 249, https://doi.org/10.1038/s41467-024-55603-1, 2025.

Nair, H., Summers, M. E., Miller, C. E., and Yung, Y. L.: Isotopic fractionation of methane in the martian atmosphere, Icarus, 175, 32–35, https://doi.org/https://doi.org/10.1016/j.icarus.2004.10.018, 2005.

Nicely, J. M., Salawitch, R. J., Canty, T., Anderson, D. C., Arnold, S. R., Chipperfield, M. P., Emmons, L. K., Flemming, J., Huijnen, V., Kinnison, D. E., Lamarque, J.-F., Mao, J., Monks, S. A., Steenrod, S. D., Tilmes, S., and Turquety, S.: Quantifying the causes of differences in tropospheric OH within global models, Journal of Geophysical Research: Atmospheres, 122, 1983–2007, https://doi.org/10.1002/2016JD026239, 2017.

Nisbet, E. G., Manning, M. R., Dlugokencky, E. J., Fisher, R. E., Lowry, D., Michel, S. E., Myhre, C. L., Platt, S. M., Allen, G., Bousquet, P., Brownlow, R., Cain, M., France, J. L., Hermansen, O., Hossaini, R., Jones, A. E., Levin, I., Manning, A. C., Myhre, G., Pyle, J. A.,

https://doi.org/10.5194/egusphere-2026-7081
Preprint. Discussion started: 26 November 2026
© Author(s) 2026. CC BY 4.0 License.

Vaughn, B. H., Warwick, N. J., and White, J. W. C.: Very Strong Atmospheric Methane Growth in the 4 Years 2014-2017: Implications for the Paris Agreement, Global Biogeochemical Cycles, 33, 318–342, https://doi.org/10.1029/2018GB006009, 2019.

Nützel, M., Stecher, L., Jöckel, P., Winterstein, F., Dameris, M., Ponater, M., Graf, P., and Kunze, M.: Updating the radiation infrastructure in MESSy (based on MESSy version 2.55), Geoscientific Model Development, 17, 5821–5849, https://doi.org/10.5194/gmd-17-5821-2024, 2024.

Oh, Y., Zhuang, Q., Welp, L. R., Liu, L., Lan, X., Basu, S., Dlugokencky, E. J., Bruhwiler, L., Miller, J. B., Michel, S. E., Schwietzke, S., Tans, P., Ciais, P., and Chanton, J. P.: Improved global wetland carbon isotopic signatures support post-2006 microbial methane emission increase, Communications Earth & Environment, 3, 159, https://doi.org/10.1038/s43247-022-00488-5, 2022.

Poulter, B., Bousquet, P., Canadell, J. G., Ciais, P., Peregon, A., Saunois, M., Arora, V. K., Beerling, D. J., Brovkin, V., Jones, C. D., Joos, F., Gedney, N., Ito, A., Kleinen, T., Koven, C. D., McDonald, K., Melton, J. R., Peng, C., Peng, S., Prigent, C., Schroeder, R., Riley, W. J., Saito, M., Spahni, R., Tian, H., Taylor, L., Viovy, N., Wilton, D., Wiltshire, A., Xu, X., Zhang, B., Zhang, Z., and Zhu, Q.: Global wetland contribution to 2000-2012 atmospheric methane growth rate dynamics, Environmental Research Letters, 12, 094 013, https://doi.org/10.1088/1748-9326/aa8391, 2017.

Quay, P., Stutsman, J., Wilbur, D., Snover, A., Dlugokencky, E., and Brown, T.: The isotopic composition of atmospheric methane, Global Biogeochemical Cycles, 13, 445–461, https://doi.org/10.1029/1998GB900006, 1999.

Randerson, J., Van Der Werft, G., Giglio, L., Collatz, G., and Kasibhatla, P.: Global Fire Emissions Database, Version 4.1 (GFEDv4), https://doi.org/10.3334/ORNLDAAC/1293, 2017.

Randerson, J. T., van der Werf, G. R., Collatz, G. J., Giglio, L., Still, C. J., Kasibhatla, P., Miller, J. B., White, J. W. C., DeFries, R. S., and Kasischke, E. S.: Fire emissions from C3 and C4 vegetation and their influence on interannual variability of atmospheric CO_2 and $\delta^{13}CO_2$, Global Biogeochemical Cycles, 19, https://doi.org/10.1029/2004GB002366, 2005.

Riddell-Young, B., Lan, X., Sherwood, O. A., S, S., and NOAA Global Monitoring Laboratory: Global Inventory of Fossil and Non-fossil Methane δ^{13}C and δD Source Signature Measurements for Improved Atmospheric Modeling, version 2025, [Data set]. NOAA Global Monitoring Laboratory., https://doi.org/10.15138/92GG-EY58, 2025a.

Riddell-Young, B., Michel, S. E., Lan, X., Tans, P., Röckmann, T., Dasgupta, B., Oh, Y., Bruhwiler, L. M. P., Fujita, R., Umezawa, T., Morimoto, S., and Miller, J. B.: Microbial driver of 2006 – 2003 CH_4 growth indicated by trends in atmospheric δD-CH_4 and δ^{13}C-CH_4, Proceedings of the National Academy of Sciences, 122, e2516543 122, https://doi.org/10.1073/pnas.2516543122, 2025b.

Rigby, M., Montzka, S. A., Prinn, R. G., White, J. W. C., Young, D., O'Doherty, S., Lunt, M. F., Ganesan, A. L., Manning, A. J., Simmonds, P. G., Salameh, P. K., Harth, C. M., Mühle, J., Weiss, R. F., Fraser, P. J., Steele, L. P., Krummel, P. B., McCulloch, A., and Park, S.: Role of atmospheric oxidation in recent methane growth, Proceedings of the National Academy of Sciences, 114, 5373–5377, https://doi.org/10.1073/pnas.1616426114, 2017.

Röckmann, T., Brass, M., Borchers, R., and Engel, A.: The isotopic composition of methane in the stratosphere: high-altitude balloon sample measurements, Atmospheric Chemistry and Physics, 11, 13 287–13 304, https://doi.org/10.5194/acp-11-13287-2011, 2011.

Roeckner, E., Brokopf, R., Esch, M., Giorgetta, M., Hagemann, S., Kornblueh, L., Manzini, E., Schlese, U., and Schulzweida, U.: Sensitivity of Simulated Climate to Horizontal and Vertical Resolution in the ECHAM5 Atmosphere Model, Journal of Climate, 19, 3771–3791, https://doi.org/10.1175/JCLI3824.1, 2006.

Sander, R., Jöckel, P., Kirner, O., Kunert, A. T., Landgraf, J., and Pozzer, A.: The photolysis module JVAL-14, compatible with the MESSy standard, and the JVal PreProcessor (JVPP), Geoscientific Model Development, 7, 2653–2662, https://doi.org/10.5194/gmd-7-2653-2014, 2014.

https://doi.org/10.5194/egusphere-2026-7081
Preprint. Discussion started: 26 November 2026
© Author(s) 2026. CC BY 4.0 License.



Saueressig, G., Bergamaschi, P., Crowley, J. N., Fischer, H., and Harris, G. W.: Carbon kinetic isotope effect in the reaction of CH_4 with Cl atoms, Geophysical Research Letters, 22, 1225–1228, https://doi.org/10.1029/95GL00881, 1995.

Saueressig, G., Bergamaschi, P., Crowley, J. N., Fischer, H., and Harris, G. W.: D/H kinetic isotope effect in the reaction $CH_4 + Cl$, Geophysical Research Letters, 23, 3619–3622, https://doi.org/10.1029/96GL03292, 1996.

Saueressig, G., Crowley, J. N., Bergamaschi, P., Brühl, C., Brenninkmeijer, C. A. M., and Fischer, H.: Carbon 13 and D kinetic isotope effects in the reactions of CH_4 with $O(^1D)$ and OH: New laboratory measurements and their implications for the isotopic composition of stratospheric methane, Journal of Geophysical Research: Atmospheres, 106, 23 127–23 138, https://doi.org/10.1029/2000JD000120, 2001.

Saunois, M., Stavert, A. R., Poulter, B., Bousquet, P., Canadell, J. G., Jackson, R. B., Raymond, P. A., Dlugokencky, E. J., Houweling, S., Patra, P. K., Ciais, P., Arora, V. K., Bastviken, D., Bergamaschi, P., Blake, D. R., Brailsford, G., Bruhwiler, L., Carlson, K. M., Carrol, M., Castaldi, S., Chandra, N., Crevoisier, C., Crill, P. M., Covey, K., Curry, C. L., Etiope, G., Frankenberg, C., Gedney, N., Hegglin, M. I., Höglund-Isaksson, L., Hugelius, G., Ishizawa, M., Ito, A., Janssens-Maenhout, G., Jensen, K. M., Joos, F., Kleinen, T., Krummel, P. B., Langenfelds, R. L., Laruelle, G. G., Liu, L., Machida, T., Maksyutov, S., McDonald, K. C., McNorton, J., Miller, P. A., Melton, J. R., Morino, I., Müller, J., Murguia-Flores, F., Naik, V., Niwa, Y., Noce, S., O'Doherty, S., Parker, R. J., Peng, C., Peng, S., Peters, G. P., Prigent, C., Prinn, R., Ramonet, M., Regnier, P., Riley, W. J., Rosentreter, J. A., Segers, A., Simpson, I. J., Shi, H., Smith, S. J., Steele, L. P., Thornton, B. F., Tian, H., Tohjima, Y., Tubiello, F. N., Tsuruta, A., Viovy, N., Voulgarakis, A., Weber, T. S., van Weele, M., van der Werf, G. R., Weiss, R. F., Worthy, D., Wunch, D., Yin, Y., Yoshida, Y., Zhang, W., Zhang, Z., Zhao, Y., Zheng, B., Zhu, Q., Zhu, Q., and Zhuang, Q.: The Global Methane Budget 2000–2017, Earth System Science Data, 12, 1561–1623, https://doi.org/10.5194/essd-12-1561-2020, 2020.

Saunois, M., Martinez, A., Poulter, B., Zhang, Z., Raymond, P. A., Regnier, P., Canadell, J. G., Jackson, R. B., Patra, P. K., Bousquet, P., Ciais, P., Dlugokencky, E. J., Lan, X., Allen, G. H., Bastviken, D., Beerling, D. J., Belikov, D. A., Blake, D. R., Castaldi, S., Crippa, M., Deemer, B. R., Dennison, F., Etiope, G., Gedney, N., Höglund-Isaksson, L., Holgerson, M. A., Hopcroft, P. O., Hugelius, G., Ito, A., Jain, A. K., Janardanan, R., Johnson, M. S., Kleinen, T., Krummel, P. B., Lauerwald, R., Li, T., Liu, X., McDonald, K. C., Melton, J. R., Mühle, J., Müller, J., Murguia-Flores, F., Niwa, Y., Noce, S., Pan, S., Parker, R. J., Peng, C., Ramonet, M., Riley, W. J., Rocher-Ros, G., Rosentreter, J. A., Sasakawa, M., Segers, A., Smith, S. J., Stanley, E. H., Thanwerdas, J., Tian, H., Tsuruta, A., Tubiello, F. N., Weber, T. S., van der Werf, G. R., Worthy, D. E. J., Xi, Y., Yoshida, Y., Zhang, W., Zheng, B., Zhu, Q., Zhu, Q., and Zhuang, Q.: Global Methane Budget 2000–2020, Earth System Science Data, 17, 1873–1958, https://doi.org/10.5194/essd-17-1873-2025, 2025.

Schaefer, H., Fletcher, S. E. M., Veidt, C., Lassey, K. R., Brailsford, G. W., Bromley, T. M., Dlugokencky, E. J., Michel, S. E., Miller, J. B., Levin, I., Lowe, D. C., Martin, R. J., Vaughn, B. H., and White, J. W. C.: A 21st-century shift from fossil-fuel to biogenic methane emissions indicated by $^{13}CH_4$, Science, 352, 80–84, https://doi.org/10.1126/science.aad2705, 2016.

Schwietzke, S., Sherwood, O., Bruhwiler, L., Miller, J., Etiope, G., Dlugokencky, E., Englund Michel, S., A. Arling, V., Vaughn, B., White, J., and P. Tans, P.: Upward revision of global fossil fuel methane emissions based on isotope database, Nature, 538, 88–91, https://doi.org/10.1038/nature19797, 2016.

Sherwood, O. A., Schwietzke, S., Arling, V. A., and Etiope, G.: Global Inventory of Gas Geochemistry Data from Fossil Fuel, Microbial and Burning Sources, version 2017, Earth System Science Data, 9, 639–656, https://doi.org/10.5194/essd-9-639-2017, 2017a.

Sherwood, O. A., Schwietzke, S., Arling, V. A., and Etiope, G.: Global Inventory of Gas Geochemistry Data from Fossil Fuel, Microbial and Biomass Burning Sources, version 2017 [data set], https://doi.org/10.15138/G3201T, 2017b.

https://doi.org/10.5194/egusphere-2026-7081
Preprint. Discussion started: 26 November 2026
© Author(s) 2026. CC BY 4.0 License.

Snover, A. and Quay, P.: Hydrogen and carbon kinetic isotope effects during soil uptake of atmospheric methane, Global Biogeochemical Cycles, 14(1), https://doi.org/10.1029/1999GB900089, 2000.

Spahni, R., Wania, R., Neef, L., van Weele, M., Pison, I., Bousquet, P., Frankenberg, C., Foster, P. N., Joos, F., Prentice, I. C., and van Velthoven, P.: Constraining global methane emissions and uptake by ecosystems, Biogeosciences, 8, 1643–1665, https://doi.org/10.5194/bg-8-1643-2011, 2011.

Still, C., Berry, J., Collatz, G., and DeFries, R.: ISLSCP II C4 Vegetation Percentage. Available on-line [http://daac.ornl.gov/] from Oak Ridge National Laboratory Distributed Active Archive Center, Oak Ridge, Tennessee, USA., https://doi.org/10.3334/ORNLDAAC/932, 2009.

Thanwerdas, J., Saunois, M., Pison, I., Hauglustaine, D., Berchet, A., Baier, B., Sweeney, C., and Bousquet, P.: How do Cl concentrations matter for the simulation of CH_4 and $\delta^{13}C(CH_4)$ and estimation of the CH_4 budget through atmospheric inversions?, Atmospheric Chemistry and Physics, 22, 15 489–15 508, https://doi.org/10.5194/acp-22-15489-2022, 2022.

Thanwerdas, J., Saunois, M., Berchet, A., Pison, I., and Bousquet, P.: Investigation of the renewed methane growth post-2007 with high-resolution 3-D variational inverse modeling and isotopic constraints, Atmospheric Chemistry and Physics, 24, 2129–2167, https://doi.org/10.5194/acp-24-2129-2024, 2024.

Thompson, R. L., Stohl, A., Zhou, L. X., Dlugokencky, E., Fukuyama, Y., Tohjima, Y., Kim, S.-Y., Lee, H., Nisbet, E. G., Fisher, R. E., Lowry, D., Weiss, R. F., Prinn, R. G., O'Doherty, S., Young, D., and White, J. W. C.: Methane emissions in East Asia for 2000–2011 estimated using an atmospheric Bayesian inversion, Journal of Geophysical Research: Atmospheres, 120, 4352–4369, https://doi.org/10.1002/2014JD022394, 2015.

Thompson, R. L., Montzka, S. A., Vollmer, M. K., Arduini, J., Crotwell, M., Krummel, P. B., Lunder, C., Mühle, J., O'Doherty, S., Prinn, R. G., Reimann, S., Vimont, I., Wang, H., Weiss, R. F., and Young, D.: Estimation of the atmospheric hydroxyl radical oxidative capacity using multiple hydrofluorocarbons (HFCs), Atmospheric Chemistry and Physics, 24, 1415–1427, https://doi.org/10.5194/acp-24-1415-2024, 2024.

Turner, A. J., Frankenberg, C., Wennberg, P. O., and Jacob, D. J.: Ambiguity in the causes for decadal trends in atmospheric methane and hydroxyl, Proceedings of the National Academy of Sciences, 114, 5367–5372, https://doi.org/10.1073/pnas.1616020114, 2017.

van der Werf, G. R., Randerson, J. T., Giglio, L., van Leeuwen, T. T., Chen, Y., Rogers, B. M., Mu, M., van Marle, M. J. E., Morton, D. C., Collatz, G. J., and Yokelson, R. J. Kasibhatla, P. S.: Global fire emissions estimates during 1997 – 2016, Earth System Science Data, 9, 697 – 720, https://doi.org/10.5194/essd-9-697-2017, 2017.

van Herpen, M. M. J. W., Li, Q., Saiz-Lopez, A., Liisberg, J. B., Röckmann, T., Cuevas, C. A., Fernandez, R. P., Mak, J. E., Mahowald, N. M., Hess, P., Meidan, D., Stuut, J.-B. W., and Johnson, M. S.: Photocatalytic chlorine atom production on mineral dust–sea spray aerosols over the North Atlantic, Proceedings of the National Academy of Sciences, 120, e2303974 120, https://doi.org/10.1073/pnas.2303974120, 2023.

Warwick, N. J., Cain, M. L., Fisher, R., France, J. L., Lowry, D., Michel, S. E., Nisbet, E. G., Vaughn, B. H., White, J. W. C., and Pyle, J. A.: Using $\delta^{13}C$-CH_4 and δD-CH_4 to constrain Arctic methane emissions, Atmospheric Chemistry and Physics, 16, 14 891–14 908, https://doi.org/10.5194/acp-16-14891-2016, 2016.

Werner, R. A. and Brand, W. A.: Referencing strategies and techniques in stable isotope ratio analysis, Rapid Communications in Mass Spectrometry, 15, 501–519, https://doi.org/10.1002/rcm.258, 2001.

Whitehill, A. R., Joelsson, L. M. T., Schmidt, J. A., Wang, D. T., Johnson, M. S., and Ono, S.: Clumped isotope effects during OH and Cl oxidation of methane, Geochimica et Cosmochimica Acta, 196, 307–325, https://doi.org/10.1016/j.gca.2016.09.012, 2017.

https://doi.org/10.5194/egusphere-2026-7081
Preprint. Discussion started: 26 November 2026
© Author(s) 2026. CC BY 4.0 License.



Whiticar, M., Faber, E., and Schoell, M.: Biogenic methane formation in marine and freshwater environments: CO_2 reduction vs. acetate fermentation—Isotope evidence, Geochimica et Cosmochimica Acta, 50, 693–709, https://doi.org/10.1016/0016-7037(86)90346-7, 1986.

Whiticar, M. J.: Carbon and hydrogen isotope systematics of bacterial formation and oxidation of methane, Chemical Geology, 161, 291 – 314, https://doi.org/10.1016/S0009-2541(99)00092-3, 1999.

Winterstein, F. and Jöckel, P.: Methane chemistry in a nutshell – the new submodels CH4 (v1.0) and TRSYNC (v1.0) in MESSy (v2.54.0), Geoscientific Model Development, 14, 661–674, https://doi.org/10.5194/gmd-14-661-2021, 2021.

Worden, J., Bloom, A., and Pandey, S. e. a.: Reduced biomass burning emissions reconcile conflicting estimates of the post-2006 atmospheric methane budget., Nature Communications, 8, https://doi.org/10.1038/s41467-017-02246-0, 2017.

Zazzeri, G., Lowry, D., Fisher, R. E., France, J. L., Lanoisellé, M., Kelly, B. F. J., Necki, J. M., Iverach, C. P., Ginty, E., Zimnoch, M., Jasek, A., and Nisbet, E. G.: Carbon isotopic signature of coal-derived methane emissions to the atmosphere: from coalification to alteration, Atmospheric Chemistry and Physics, 16, 13 669–13 680, https://doi.org/10.5194/acp-16-13669-2016, 2016.

Zhang, J., Qiu, B., Khanna, N., and Lin, J.: Regional production shift and increased utilization dampen the growth of China's coal mine methane emissions, Communications Earth & Environment, 6, 964, https://doi.org/10.1038/s43247-025-02922-w, 2025.

Zhao, Y., Saunois, M., Bousquet, P., Lin, X., Berchet, A., Hegglin, M. I., Canadell, J. G., Jackson, R. B., Dlugokencky, E. J., Langenfelds, R. L., Ramonet, M., Worthy, D., and Zheng, B.: Influences of hydroxyl radicals (OH) on top-down estimates of the global and regional methane budgets, Atmospheric Chemistry and Physics, 20, 9525–9546, https://doi.org/10.5194/acp-20-9525-2020, 2020.